

Response of silicon nitride ceramics subject to laser shock treatment

Shukla, P., Shen, X., Allott, R., Ertel, K., Robertson, S., Crookes, R., Wu, H., Zammit, A., Swanson, P. & Fitzpatrick, M. E.

Author post-print (accepted) deposited by Coventry University's Repository

Original citation & hyperlink:

Shukla, P, Shen, X, Allott, R, Ertel, K, Robertson, S, Crookes, R, Wu, H, Zammit, A, Swanson, P & Fitzpatrick, ME 2021, 'Response of silicon nitride ceramics subject to laser shock treatment', *Ceramics International*, vol. 47, no. 24, pp. 34538-34553.

<https://dx.doi.org/10.1016/j.ceramint.2021.08.369>

DOI 10.1016/j.ceramint.2021.08.369

ISSN 0272-8842

Publisher: Elsevier

NOTICE: this is the author's version of a work that was accepted for publication in *Ceramics International*. Changes resulting from the publishing process, such as peer review, editing, corrections, structural formatting, and other quality control mechanisms may not be reflected in this document. Changes may have been made to this work since it was submitted for publication. A definitive version was subsequently published in *Ceramics International*, 47:24, (2021) DOI: 10.1016/j.ceramint.2021.08.369

© 2021, Elsevier. Licensed under the Creative Commons Attribution-NonCommercial-NoDerivatives 4.0 International <http://creativecommons.org/licenses/by-nc-nd/4.0/>

Copyright © and Moral Rights are retained by the author(s) and/ or other copyright owners. A copy can be downloaded for personal non-commercial research or study, without prior permission or charge. This item cannot be reproduced or quoted extensively from without first obtaining permission in writing from the copyright holder(s). The content must not be changed in any way or sold commercially in any format or medium without the formal permission of the copyright holders.

This document is the author's post-print version, incorporating any revisions agreed during the peer-review process. Some differences between the published version and this version may remain and you are advised to consult the published version if you wish to cite from it.

Response of Silicon Nitride Ceramics subject to Laser Shock Treatment

P. Shukla^{*1}, X. Shen¹, Ric Allott², Klaus Ertel², S. Robertson³, R. Crookes³, H. Wu³,
A. Zammit⁴, P. Swanson¹ and M. E. Fitzpatrick¹.

^{*1}School of Mechanical, Aerospace and Automotive Engineering, Coventry University, Priory Street, Coventry, CV1 5FB, United Kingdom.

²Central Laser Facility, STFC Rutherford Appleton Laboratory, Harwell Campus, Didcot, OX11 0QX, UK.

³Department of Materials, Loughborough University, Loughborough, LE11 3TU, United Kingdom

⁴Department of Metallurgy and Materials Engineering, Faculty of Engineering, University of Malta, Msida, MSD2080, Malta

Abstract

A comprehensive and novel investigation on multiple-layer, square-beam laser shock treatment (“laser peening”) of Si_3N_4 ceramics is reported in this work. Surface topography, hardness, fracture toughness (K_{IC}), residual stresses, and microstructural changes were investigated. The evaluation of fracture toughness via the Vickers hardness indentation method revealed a reduction in crack lengths produced by the indenter after laser shock treatment. Upon appropriate calculation, this revealed an increase in K_{IC} of 60%, this being attributed to a near-surface (50 μm depth) compressive residual stress measured at –289 MPa. Multiple layer laser shock treatment also induced beneficial residual stresses to a maximum measured depth of 512 μm . Oxidation was evident only on the top surface of the ceramic post laser shock treatment (<5 μm depth) and was postulated to be due to hydrolyzation. The surface enhancement in K_{IC} and flaw-size reduction was assigned to an elemental change on the surface, whereby, Si_3N_4 was transformed to SiO_2 , particularly, with multiple layers laser shock treatment. Compressive residual stresses measured in the sub-surface (512 μm) were due attributed to mechanical effects (below sub-surface elastic constraint) and corresponding shock-wave response of the Si_3N_4 . This work has led to a new mechanistic understanding regarding the response of Si_3N_4 ceramics subject to laser shock treatment (LST). It is significant because inducing deep compressive residual stresses and corresponding enhancement in surface K_{IC} are important for the longevity enhanced durability in many applications of this ceramic including cutting tools, hip and knee implants, dental replacements, bullet-proof vests and rocket nozzles in automotive, aerospace, space and biomedical industries.

Keywords: Laser Peening; ceramics; Silicon Nitride; Strengthening; Residual Stress; Microstructure; Shock Treatment.

1. Introduction

1.1 Background of Si_3N_4 Ceramics

Si_3N_4 ceramic is widely applied in industry from the family of advanced ceramics [1-3]. Compared to other ceramics, a Si_3N_4 is a very stable material, with high hardness, very good wear resistance, along with anti-bacterial properties and hydrophilicity [4]. Si_3N_4 is also dense and light-weight, has good corrosion properties, but has relatively low fracture toughness (K_{Ic}) [4, 5]. Some of the industrial application of Si_3N_4 are: cutting tools; valves; pistons; exhaust manifolds; seals; turbo chargers; bearings; turbine blades; and rocket nozzles and rotors [4]. Other applications span from ball and socket joints, hip and knee implants, dental replacements, to bullet-proof vests and body/vehicle armours, sensors for detecting motion and energy storage components in electric vehicles. For such applications, enhancing the mechanical properties is highly beneficial as it leads to better functional performance and improved service life.

Crack sensitivity and low K_{Ic} can limit the use of Si_3N_4 , particularly, for demanding applications. Nevertheless, the applications of Si_3N_4 have gradually increased on account of the desirable physical properties and longer functional life which often gives Si_3N_4 a commercial advantage over the conventional materials in use. With that said, not only Si_3N_4 but ceramics in general show limited plasticity and deformation when exposed to an external stimulus such as pressure *via* mechanical pre-stressing, although, there is ongoing research to extend further, the limited available plastic deformation in hard brittle ceramics [6, 7]. Nishimura et al. [8] reduced the grain particle size of Si_3N_4 ceramic with sintering at 1450°C to 1600°C, with additives Y_2O_3 , Al_2O_3 , and MgO by high-energy end-milling. This reduced the particle size and nano-meter sized grains were obtained. These workers reported that brittle ceramics can be deformed plastically at the same level of their sintering temperature, when grain size is made sufficiently small [8], implying grain boundary sliding sourced plasticity.

In Al_2O_3 ceramics, a glassy amorphous phase was reported at the grain boundaries [9]. Shock-induced spall was reported in single and nanocrystalline SiC by Li *et. al.* [10].

Superplasticity, with a large elongation during tensile deformation was reported by Chen and Xue [11] in ZrO_2 , Si_3N_4 and Al_2O_3 and their composites. This was obtained by designing the microstructures of the ceramics with ultra-fine-grains that are stable and resistant to coarsening during sintering and deformation. A low sintering temperature is required, and an appropriate phase selection required, specifically, the tetragonal phase in zirconia or the alpha phase in Si_3N_4 , that in turn, prevents grain growth. A second-phase is also useful in stopping static and dynamic grain growth and in addition to maintaining an adequate grain-boundary cohesive strength, relative to the flow stress, will mitigate cavitation or grain-boundary cracking during large strain deformation [11]. Moreover, superplastic behaviour was also reported in composites of fine-grained monolithic SiC/ Si_3N_4 (SiAlON) at temperatures ranging from 1450°C to 1650°C, at strain rates between 10^{-5} and $10^{-4} s^{-1}$ [12]. Super-plasticity is however, common in many metals and alloys, but has also been reported in ceramics extensively [13 - 15]. It occurs when the grain size is refined smaller than a few micrometres, whilst, the deformation temperature is above two-thirds of the melting-point [13].

The laser shock treatment (LST) technique applied here, inspired from laser shock peening (LSP), is, however, a cold process and generates low thermal input into the material being applied at room temperatures. Hence, super-plasticity in the absence of an, additional heat source will not take place, and inducing any plastic deformation at room temperature proves to be challenging, given to the fact that polycrystalline ceramics have little or no plasticity, due to the nature of their fundamental (ionic or covalent) atomic bonding. Having said that, plasticity was reported in a ZrO_2 micropillars in a compression test at room temperature [16].

Kiani *et al.* [17], localised plasticity with dislocation activity in a single crystal 6H-SiC. Basal-plane dislocations less line was than of line length circa 300nm were reported in single-crystal SiC micropillars. The applied stress was around 7.8GPa. Comparatively, this type of stress in the form of pressure pulses can easily be achieved with a nano-second laser of several joules of laser pulse energy. During the peening process localized, plasticity may be

evidenced by laser-plasma driven shock-waves, interacting with the surface and sub-surface of the Si_3N_4 ceramics and create ultra-high strain-rates, **surface local** plastic deformation, and **consequent** compressive residual stress (**due to elastic constraint imposed by the underlying un-shocked material**) as one potential mechanism. It is therefore, possible that LSS can be beneficial in obtaining a level of plasticity that is desirable for industrial ceramic components. Longy and Cagnoux [18] found dislocation twins were generated due to high velocity impacts on Al_2O_3 armour.

Grinding and polishing Al_2O_3 matrix composites found strength enhancements in the work of Wu *et al.* [19]. Bhattacharya *et al.* [20] reported, deformation of alumina at high strain-rates, stating that plasticity leads to increased dislocation activity **associated with** compressive behaviour in brittle materials [20]. Bhattacharya *et al.* studied the compressive failure mechanisms at low strain-rates in a coarse-grained alumina ceramic. About 40% enhancement in compressive stress bearing capability was found with increased strain, dislocation presence and micro-plasticity evidenced. Using fluorescence microscopy, Wu *et al.* measured the residual stress distribution around an indentation and scratches in a polycrystalline Al_2O_3 and $\text{Al}_2\text{O}_3/\text{SiC}$ nanocomposite [21 -22].

1.2 State-of-the-art in Peening Advanced Ceramics

Lasers are known to influence the surface properties of ceramic materials in general [5]. Laser Shock Peening (LSP), has been an established technique for number of years for the surface treatment of metals in particular [23 - 29]. However, LSP of advanced ceramics is still an under-developed process for a number of reasons [30], such as the physical characteristics that prevent ceramics from behaving in the same way as metals when exposed to short-pulses of laser energy. Thus, mechanical yielding and plastic deformation within ceramics is difficult to **induce**. Therefore, the same benefits and mechanisms **associated with LSP of** metals are not common with hard, brittle ceramic materials.

A successful technique to surface engineer advanced ceramics would open new avenues for their use in demanding applications. Typical ceramic products in engineering, such as, high-performance cutting tools; knives, and machine tools could benefit from LSS. Bulk metallic glass ($Zr_{41.2}Ti_{13.8}Cu_{10}Ni_{12.5}Be_{22.5}$ (vit1)) was laser peened by Zhu *et al.* [28] who reported that LSP increased surface roughness and hardness decreased by up to 13%. The softening effect was attributed to the high-density shear-bands induced by the LSP.

Koichi *et al.* [31], investigated laser peening of Si_3N_4 ceramics. Microstructural modifications were not reported, however, observed, plastic deformation was reported, based on flexural strength test and fracture toughness data. In a feasibility study, heat-assisted laser shock peening of a single silicon crystal was also reported by Cheng *et al.* [32]; It was demonstrated that large compressive residual stresses can be introduced in the magnitude of 3.2GPa on the surface and about 0.5GPa, below the surface via plastic deformation facilitated dislocation activity; [32]. Our recent studies on laser peening Al_2O_3 and Si_3N_4 ceramics also showed modification in hardness and fracture toughness (K_{Ic}) [33 – 35]. Surface property modification of SiC can be induced by LSP with the magnitude of surface compressive stress being dependent on laser intensities [36]. Laser shock peening using selected parameters was conducted for an Al_2O_3 armour ceramic [37], which rendered up to -200 MPa of compressive residual stress, the material's fracture strength increased, and dislocation density was enhanced [38]. Wang *et al.* investigated laser shock processing of alumina ceramics from a mechanistic view-point [39 - 41], addressing changes in properties associated with dislocation activities. Having said that, it is still unclear how consistent their laser shock processing technique was, when applied over the Al_2O_3 and SiC ceramics when viewing surfaces at macroscale, with respect to producing crack-free features on a particular given area over the samples.

Saigusa *et al.* [43], investigated the feasibility of laser peening silicon nitride reinforced with silicon carbide (Si_3N_4/SiC) and compared it with shot peening and found up to 230 MPa

of compressive residual stress at a depth of about 50 μ m. They reported that the magnitude of the surface residual stress of the laser-peened specimen was smaller than **from** shot-peening on the Si₃N₄/SiC, but laser peening introduced a deeper compressive residual stress. However, this study did not show fundamental effects of material characteristics in terms of property, microstructure and the mechanism during LSS.

Sekine *et. al.* [42], shock compressed β - Si₃N₄ powders by a quenching process generating compressive residual stresses, ranging from 12 to 115 GPa. As result β - Si₃N₄, transformed to the spinel c- Si₃N₄ at pressures above about 20GPa. This was classified as a fast re-constructive method. Using this technique, it was demonstrated that mechanical properties can be tailored to suit industrial applications. Laser shock peening induces laser plasma-driven shock-waves into the surface of metals [44], thus, it is practically possible to induce pressure in the range of 15 to 40GPa using laser shock strengthening.

1.3 Research Rationale

Pfeiffer and Frey shot peened a Si₃N₄ ceramic and reported that micro-plastic deformation can be induced into the near surface, with the prospect of dramatically increasing the strength of Si₃N₄ with an increase in fracture toughness by a factor of **x3**. Additionally, at a depth of 30 μ m, maximum compressive stresses of 2000MPa by using shot peening pressures of 0.3MPa were reported using an X-ray diffraction (XRD) method [45]. These authors also reported 1200MPa of compressive stress in Si₃N₄ at a shallow depth of 5 μ m in another investigation, for tempered (800 °C) shot peened ceramics [46]. These investigations have shown that ceramics of brittle nature such as Si₃N₄ can be strengthened with similar effects **as** are seen with metals. However, no mechanistic rationale were reported, which encouraged **d** us to observe what effects our controlled and precise LSS techniques would bring to the ceramic surface and sub-surface layer.

The conventional multiple layer peening technique utilises an ablative layer tape on the surface. As this was not the case for our study, the Si₃N₄ ceramics treated with multiple

laser shocked layers, may show additional effects from surface ablation and the possibility of receiving/responding to the shock waves with a different response – leading to different effects and a strengthening mechanism demonstrated via property and evolved microstructural changes. Moreover, we do not utilise any pre-or-post-heating of the ceramic as that is time-consuming, costly, and increases experimental constraints. This is the first-time a comprehensive investigation of the plasma-driven laser shock based method is presented for Si₃N₄ ceramic, particularly with a square laser spot “footprint”. We present an in-depth analysis of the effect of laser shock vs. Si₃N₄ material interaction properties offered.

Lastly, another motivation of this paper is the fact that alternative methods applicable for surface engineering ceramics such as Si₃N₄, namely; grinding and polishing, do not induce deep residual stresses, whilst, laser shock peening is known to achieve this with metals, specifically, due to the depth that the shockwave travels. Additionally, other methodologies such as shot peening is also not capable of performing this. In particular, fatigue in Si₃N₄ ceramic bearing can cause significant damage, thus, improving fatigue life via an advanced process such as laser shock treatment could be significantly fruitful and beneficial.

2. Materials and Methods

2.1 Details of Si₃N₄ Advanced Ceramic

A cold isotatically pressed (CIPed) Si₃N₄ advanced ceramic was obtained from Shanghai United Technology (Shanghai, China) with the dimension 50mm × 10mm × 5mm bar. The Si₃N₄ ceramic comprised 90.5wt% Si₃N₄, and 6 wt% yttria, 4 wt% unspecified content. It was CIPed at a pressure of 455 bar from all directions and sintered at 1200 °C for 5 hours to reach full densification (as specified by the manufacturer). The density of the Si₃N₄ was in the range of 3.20 - 3.30 g/cm³. The ceramic was mechanically and microstructurally characterized before all laser-based experimentation. The average as-received surface finish was Sa = 1.12 μm. The surface hardness was measured to be 1515HV using 10Kg indentation load, and plane-strain surface fracture toughness (K_{IC}) was determined to be 2.9 MPa.m^{1/2}. It is usually well known that the K_{IC} of the Si₃N₄ ceramic is between 4 to 6 MPa and the hardness is around 1600HV

$\pm 10\%$. There are many sources which we can obtain this from. We have now stated the references (sources), where the information comes from [4, 8, 35]. It is an indication of how much the experimental data obtained from the material surface is different from the conventional Si_3N_4 macroscopically measured K_{IC} as a comparison. This is naturally, somewhat, higher than the values reported in this work as we have evaluated the surface and sub-surface up to $16\mu\text{m}$ depth only.

2.2 Details of Laser Shock Treatment Applied to Si_3N_4 Ceramics

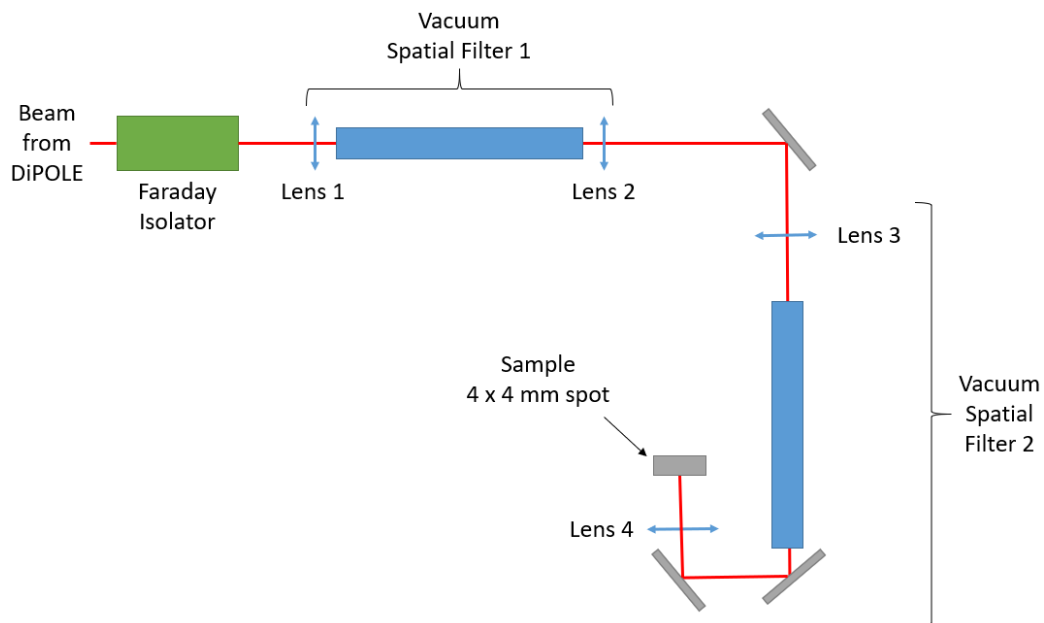
Single, double and multiple passes (layers) of laser shock treatments were applied using a pulsed 10J, 10Hz, 10ns, DiPOLE laser at the UK's Central Laser Facility (STFC). As aforementioned, the laser shock treatment was inspired by the conventional laser shock peening process. The DiPOLE system utilises a cryogenic gas-cooled amplifier head containing multi-slab Yb:YAG gain media producing a 1030nm wavelength; output pulses of 10ns at 1Hz repetition rate. were employed. Based on knowledge of laser processing ceramics, from our previous work [33 - 38], laser energy of 1J was applied with a fairly large square footprint and spot size of 4.5mm x 4.5mm. The overlap of the surface treatment was 0% to avoid any cracking being induced into the material, and due to the fact that this investigation was focused on the study of multiple layer shock peening of the Si_3N_4 ceramic.

The laser beam propagation factor M^2 was averaged at 1.4, being 1.6 in X-and 1.2 in Y-direction. The laser beam intensity delivered at the Si_3N_4 workpiece was 0.64 GW/cm^2 and the radiance density determined based on our published technique [47], equated to $2.82 \text{ W/cm}^2 \cdot \text{Sr} \cdot \mu\text{m}$ per pulse. The beam profile was flat-top ("top hat"). Parameters are summarized in further detail in Table 1. For these experiments, a black-ink layer was used to visually see the foot-print of the laser pulse on the Si_3N_4 ceramic samples. Once the beam had impacted the Si_3N_4 for the first-time (first pulse (1 layer)), the ablative ink layer was removed. Figure 1 shows a schematic of the DiPOLE laser shock peening system and beam delivery in Figure 1(a). In Figure 1(b), the schematic shows laser shock treatment applied onto the Si_3N_4 ceramic

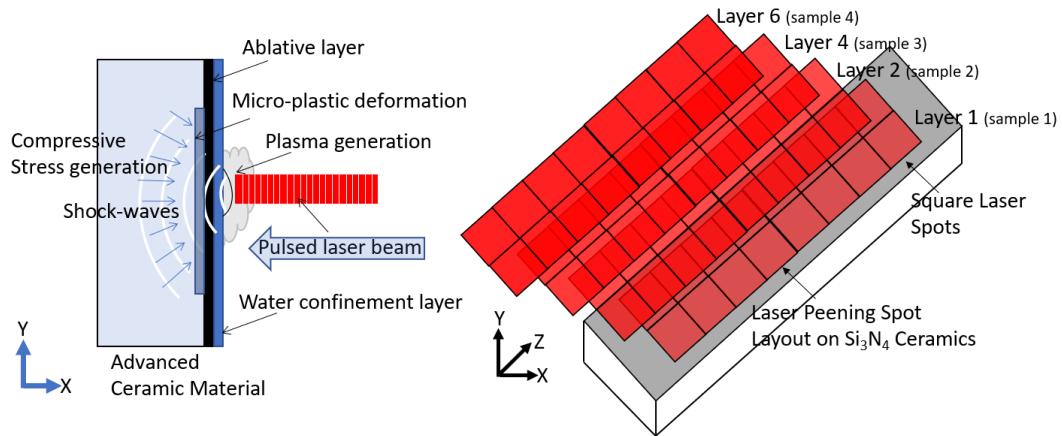
with its material response. Figure 1(c) illustrates the laser shock treated samples of the Si_3N_4 ceramics.

Table 1. Process parameters of laser shock treatment applied to Si_3N_4 Ceramics.

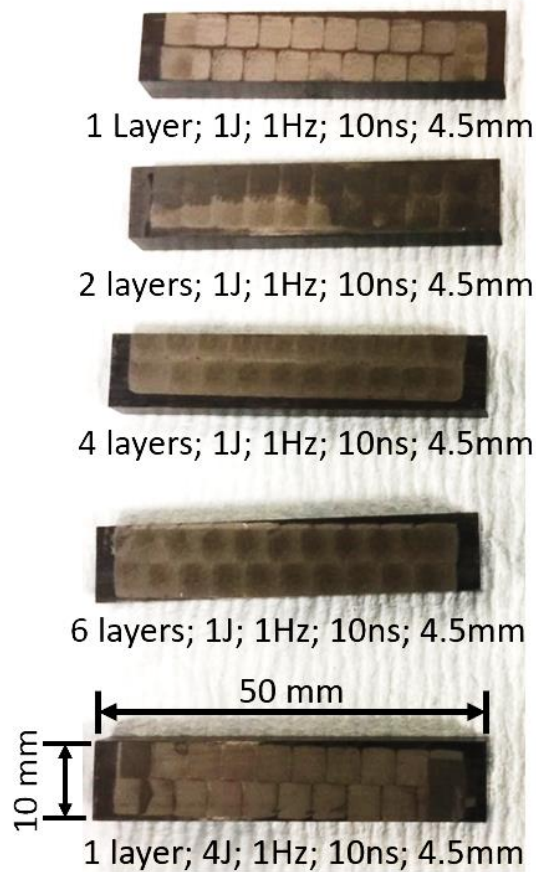
Process Parameters	
Laser Energy/J	1
Square Spot Size Dimension/mm	4.5
Laser Intensity /GW/cm ²	0.62;
Radiance Density / W.cm ² .Srt.μm	2.82;
Layers	1,2,4 or 6
HEL of Si_3N_4 /GPa	4.62
Shock Pulse Pressure/GPa	1.33/pulse
Overlapping/%	0
Pulse Repetition Rate (PRR) / Hz	10
Pulse Duration / ns	10
Beam Shape	Top-hat, Square
M^2	1.4 (1.6 in X and 1.2 in Y)



(a)



(b)



(c)

Figure 1. A schematic of the DiPOLE laser shock peening system/beam delivery in (a); a schematic of the laser shock treatment applied onto the Si₃N₄ ceramic as well as its material response in (b) and (c) the laser shock treated samples of the Si₃N₄ ceramics.

2.3 Residual Stress Analysis

2.3.1 Incremental Hole Drilling

Residual stress analysis was performed using the Incremental Centre Hole Drilling (ICHD) technique. ICHD technique is a semi-destructive stress-relaxation method that employs **the interpretation** of mechanically relaxed strains, close to the surface of a component during the drilling of a shallow, blind hole (up to 1.66 mm **depth**). The technique utilizes an inverse method for determination of the “locked-in” stresses from three components of relaxed strains. This technique is ideal for evaluating surface and sub-surface effects, providing information on shock-wave penetration as result of the LSS treatment. Measurements were carried out at the centre of each specimen. Rosette strain gauges type 062UL with an external diameter of 5.13mm were adhesively bonded on the Si₃N₄ ceramic **samples** to measure the relaxed surface strains. Then using an RS-200 milling guide, a 1.66mm diameter drill bit was used for drilling the hole at the centre of the rosette strain gauge. As a technical requirement of ICHD technique, the hole was incrementally drilled with smaller drilling depth of 32µm close to the surface and the bigger steps of 128µm were chosen for further distance from the surface, recording data to a depth of 1.024mm. The Young’s modulus of the Si₃N₄ was 320MPa and Poisson’s ratio was 0.26.

2.3.2 Residual Stress by indentation Method

The Vickers indentation method was used to determine the residual stress on the surface of both the as-received and the laser shock treated Si₃N₄ ceramics. This measured the surface and near surface stresses (under 100µm) to obtain further comparison and verification of the stresses obtained by ICHD. Vickers indentation were used to produce 10 indentations with over each sample with a load of 10Kg. Average crack lengths and the hardness, indentation size was then recorded and tabulated into Marshall and Lawn Equation [48].

$$\sigma_r = \frac{\sqrt{\pi X}}{2m\sqrt{c}} \left(\frac{K_{IC}}{c} - \frac{P}{c^{3/2}} \right) \dots \dots \dots (1)$$

Where K_{Ic} is fracture toughness ($\text{MPa}\cdot\text{m}^{0.5}$); a is crack length (m); P is the indentation load; $c = 2a$ (m), where c is the crack tip to crack tip length in metres; $m = 1$ and χ is a material and indenter dependent constant [49]:

$$\chi = 0.016 \left(\frac{E}{H}\right)^{0.5} \dots\dots\dots(2)$$

Where 0.016 is the geometrical constant, E is the Young's modulus and H is the Vickers hardness. This was implemented in the work of Rickhey *et al.* [50].

2.3.3 Residual Stress by X-ray diffraction

Surface stresses were measured using a Rigaku Ultima IV X-Ray diffractometer, set in theta-two theta configuration and using parallel beam geometry. A $\text{CuK}\alpha$ radiation source was utilised at an acceleration voltage of 45 kV and a current of 40 mA. The (303) crystal plane peak occurring at a 2θ angle of 120.4° was chosen as the reference on which the peak shift was calculated. Based on this, the 2θ range was set from 119° to 122° with a step size of 0.01° and an exposure time of 20 seconds. The $\sin^2\psi$ method was used for the measurement and the samples were tilted using a Rigaku Multipurpose attachment IV (MPA-U4). Various ψ angles ranging between 0° and 46° were used. The values of Young's Modulus and Poisson's ratio used to calculate the residual stress were 320 MPa and 0.26 respectively.

2.4 Hardness Testing and Fracture Toughness (K_{Ic}) Measurement

Hardness testing was conducted using a Mitotoyo automatic hardness tester with a Vickers diamond indenter. Following the ISO standards on hardness testing, the indentation load applied for the hardness test was 10Kg, with 10 individual diamond indentations placed at a sufficient distance adjacent to each sequential indentation in a single line for laser shock treated and the untreated Si_3N_4 (see Figure 2). The hardness tests then enabled determining the plane-strain fracture toughness (K_{Ic}) using the Vickers indentation method. The Young's

modulus used was 320GPa, with the respective hardness value for the 10 indentations on each laser shock treated and untreated Si₃N₄. An optical microscope (Lyca, Milton Keynes, UK) with its respective software was deployed for measuring the crack lengths of each Vickers indentation diamond with the use of x10 lens. To determine the K_{IC} of the Si₃N₄, the values of the crack-length were then tabulated into Equation 3, developed by Anstis and Chantikul [51]:

$$K_{1c} = 0.016 \left(\frac{E}{Hv} \right)^{0.5} \cdot \left(\frac{P}{c} \right)^{1.5} \dots\dots\dots(3)$$

Where E is the Young's modulus, HV is the **Vickers** hardness, P is the load in N, and c is the crack-length (2a) **measured from** the diamond footprint corners. This method was validated with our work for measuring the K_{IC} of laser shock treated ceramic surfaces [52]. For each surface, an average and standard deviation was calculated from 10 indentation foot-prints on each laser shock treated and untreated surface for both the hardness and K_{IC} property measurements.

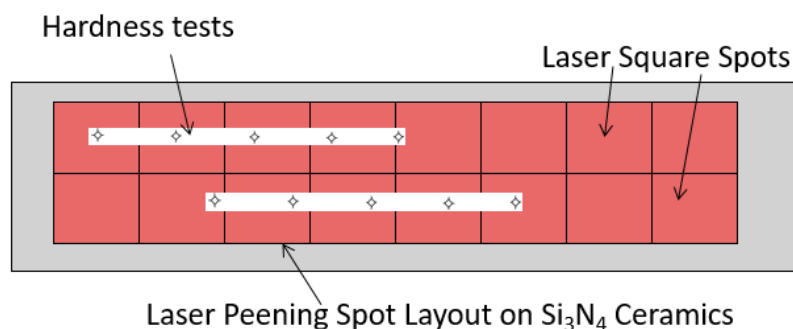


Figure 2. Illustration of the method of hardness measurement on the laser treated Si₃N₄ ceramic.

2.5 Microstructural, Elemental and Phase Analysis

Optical microscopy **at low magnifications x5 and x10** was deployed to observe and understand the effects of laser shock treatment on the Si₃N₄ ceramic **surface**. The microscope used was an upright Leica Microsystems microscope. Scanning Electron Microscopy was performed using a Zeiss, SUPRA40 for detailed high resolution imaging. Various micrographs at different magnification were taken to observe the **crack/fracture**

morphology and the surface integrity, Energy dispersive spectra (EDS) were obtained using an SEM/EDS from Thermo Fisher Scientific, Madison, WI USA. The steps (EDS conditions) taken in order to make the data as robust as possible were; 5 keV, 6.4 nA, and a process time to achieve the spectrum of 6 minutes was used with a 6 min frame time for each area at a magnification of $\times 500$. An energy resolution of 5 keV- was used to ensure surface sensitivity (300nm approx.), limit carbon contamination and improve spectral resolution to the low energy EDS lines.

A pre-tilted holder was used to “mill” the sample perpendicular to the ion beam in a field emission SEM instrument and then tilt to 54° where the sample is then planar to the EDS detector. The process time was as high as 6 minutes to ensure highest spectral resolution, and a low magnification of $\times 500$ to ensure sufficient area was sampled. It is also believed that the roughness of the sample did not affect the results. These elemental maps provide an idea of the location of the various elements. Cross-sectional maps were taken to provide the location of the various elements in the shocked subsurface. Samples were mounted on a 38° pre-tilt.

2.6 Phase Identification

Phase identification of untreated and laser shock treated samples was carried out using a Rigaku Ultima IV X-Ray diffractometer. The source of radiation was $\text{CuK}\alpha$ operated at an acceleration voltage of 45 kV and a current of 40 mA. The samples were scanned at a 2θ range between 10° and 80° using a scan speed of $1^\circ/\text{minute}$. The diffraction patterns acquired were analysed with Rigaku PDXL2 XRD analysis software and matched to PDF-4+ ICDD card library.

3. Results and Discussion

3.1 Residual Stress

3.1.1 Surface Residual Stress with Indentation Method

Table 2 presents the residual stresses measured using the **Vickers** indentation method. The depth of penetration is also shown for the respective diamond indentation. This was based on 1/7th (14%) of the total size of the diamond indentation measured [53].

The as-received surface showed compression of about -40MPa. The compressive stress after 1 layer of peening was -61 MPa and -55MPa with 2 **peening** layers applied. With that said, **samples subject to 4 peening** layers showed the lowest compressive stress of -26MPa, then the compressive stress increased to -52MPa with 6 layers applied. This meant that the only trend that can be discerned is the decreasing compressive stress as the number of **peened** layers increased.

The depth of indentation penetration for the as-received surface was over 15µm, whilst the depth of penetration was lower for the Si₃N₄ treated with 1 layer **of peening**. This increased with 2 layers, 4 layers and 6 layers in comparison, however, **the 4 layer peened surface exhibited** the lowest (15 µm) from the three. At the same time, the highest penetration was **obtained with** 6 layers (16 µm). The highest compressive stress was found in the surface treated with 1 layer, whilst the depth of indentation penetration was the lowest. What this revealed is that the surface showed much resistance to indentation response due to the compressive stress preventing the Vickers indentation **not penetrating as deep** within the Si₃N₄. Having said that the same cannot be said about the surface treated with 2 layers, as the depth of penetration is of the higher side.

So all-in-all the results from the indentation method to determine the residual stress and its depth is subjective to the indentation response which is controlled by the surface morphology, and since the surface morphology is controlled by the amount of oxidation, the stress data has not yielded a fully consistent trend using the indentation technique.

Therefore, comparing **indentation measurement sourced** residual stresses, with through thickness **residual stress values obtained** using ICHD **reveals that the** results is not akin, as the indentation method is subject to data gathered with respect to crack length and the indentation hardness. Even so, what does **correlate** is the overall nature of the results,

whereby, the trend of residual stress changing with each number of peened layers applied to a sample is in good agreement with the results further discussed of ICHD analysis. It is evident that there is some scatter in the data, however, with ceramics variation in the mechanical properties, and inhomogeneous microstructures would have likely caused this trend more frequently than metals on a batch-by-batch basis.

Table 2. Measured residual stress over the as-received and the laser shock treated Si_3N_4 ceramics via Vickers indentation method.

Sample Condition	Residual Stress / MPa		Depth of Compression / μm
	Average	STDEV	
As- received	-40	6	15 (± 5)
1 Layer, 1J	-62	7	15 (± 2)
2 Layers, 1J	-55	7	16 (± 3)
4 Layers, 1J	-27	6	16 (± 4)
6 Layers, 1J	-53	13	16 (± 1)

3.1.2. Incremental Hole Drilling (ICHD)

Figures 3(a) and (b) shows the incremental hole drilling result averages of residual stresses in X and Y directions from the as-received Si_3N_4 as well as with multiple layer treatments.

The as-received surface comprised of surface compressive stress that were measured at a depth of about $32\mu\text{m}$. As the diamond drill of the ICHD equipment penetrated deeper, the pre-existing compressive stress reduced to an average of -153 MPa . The measured stress curve for the as-received condition then proceeds into tension with increasing depth ($+160\text{ MPa}$ at $112\mu\text{m}$ depth) prior to flattening down to 0 MPa at a depth of about $512\mu\text{m}$. The curve maintained the same without any fluctuations thereafter, to a depth of $1024\mu\text{m}$.

After applying 1 layer with 1J, the sample showed tensile stress of 384 MPa on the surface up to $16\mu\text{m}$. This reduced to compressive stress of a -126 MPa at a depth of $80\mu\text{m}$.

The residual stress over the sample treated with 2 layers, 1J showed compressive stress of -163MPa (at 16 μ m depth), which then further reduced to -289MPa at 48 μ m depth prior to subsequently rising in tension at a depth of 100 μ m. The onset of stress from there on was much stable at a tensile value of 50MPa throughout the bulk.

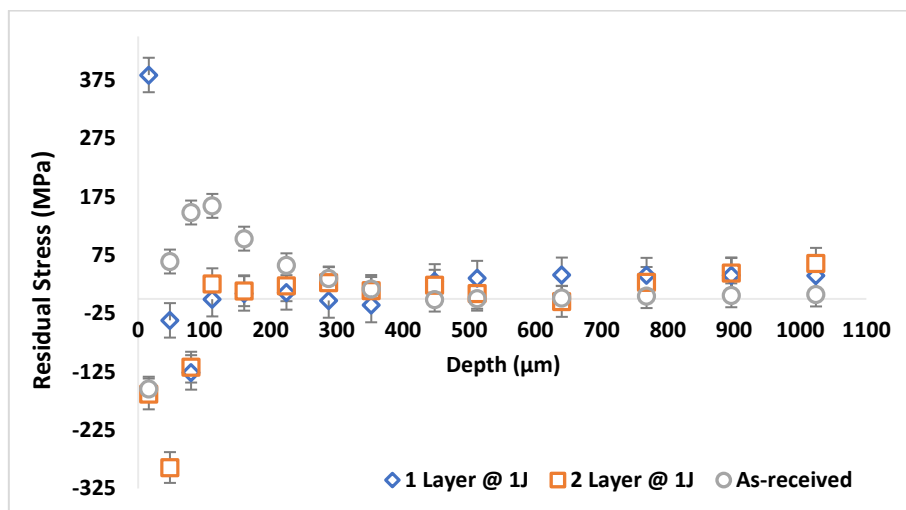
Upon applying 4 layers treatment to the Si₃N₄, the surface residual stress was compressive at -12MPa (up to 16 μ m depth), then increased to about 113MPa in tension at 80 μ m depth, and dipped down in compression to -89MPa at a depth of 160 μ m. The **sub-surface residual stress** subsequently, remained in tension through the bulk peaking at 215MPa at a depth of 640 μ m. **This was slightly higher than others samples and is subject to further repetition of test data for verification. However, based on the consistency of other data, it is postulated that a flaw in the sample (porosity or micro-cracks) may have occurred within the localised region where the ICH measurement was conducted. Thus, few points in the data, specifically, at 640 μ m to 890 μ m depth, were slightly higher, compared to the other samples.** All other measurements through the bulk of the Si₃N₄ ceramic samples were **consistent** and in good agreement. We postulate **this discrepancy** was due to the inhomogeneous microstructure, occurrence of a void or natural defects within the Si₃N₄, since the measurement technique and methods used for ICHD were identical for all the samples. Other results with the same sample also follow a similar trend.

After 6 layers were applied, the stress rose to a mean value of 47MPa at a depth of 16 μ m, the stress then progressively reducing to compressive (-49 MPa) at a depth of 160 μ m, then rising to tension at around 520 μ m depth and remained in the same state through the bulk.

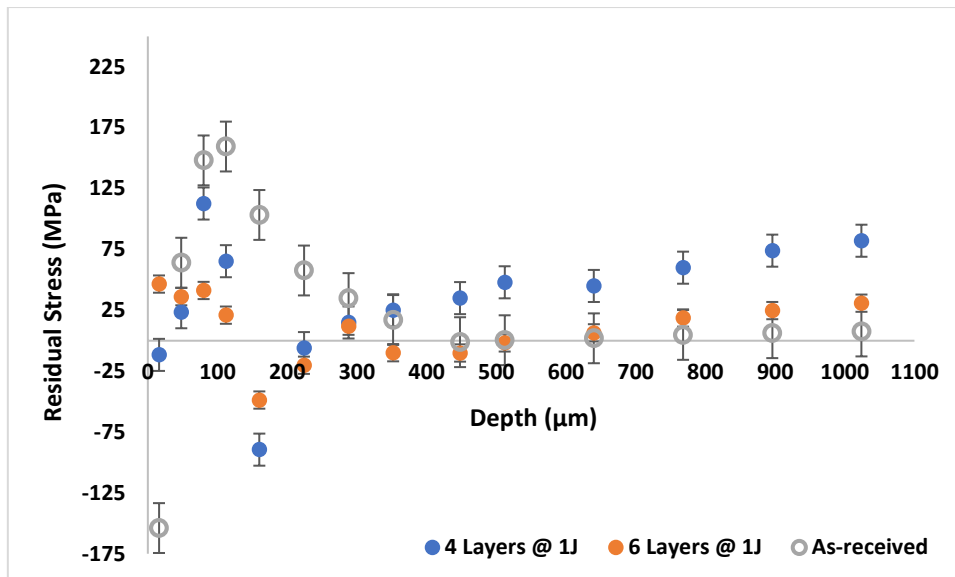
It was observed that as more layers were added, the residual stress deepened, but in turn, reduced in magnitude as the shock-waves penetrated into the bulk of the ceramic. When the laser shock treated surface was compared to the as-received surface, it was evident that the shock wave generated a **residual** stress profile that was different in both surface and the bulk. The difference was that the short-pulse laser energy, in turn,

introduced some tensile stress on the surfaces of all the laser shock treated ceramics, but as the shock-waves penetrated into the thickness, micro-plastic deformation rendered compression under the surface and compressive stress was therefore exhibited as can be seen in Figures 3(a) and (b). The compressive stress was evident more on the surface of the as-received sample. This was because of the initial cold isostatically pressed manufacturing process, which the material experienced before being exposed to laser shock treatment. This technique introduced 5 bar of pressure on the surface of the test samples from all directions and created a top layer that was measuring in compression, but then became tensile in the bulk. Laser shock treatment then changed this and induced compressive stress particularly within the sub surface (up to 300 μm) of the Si_3N_4 ceramics.

The results of the residual stress for the Si_3N_4 treated with 2 layers have shown that significant compressive stress has been induced to a depth of about 50 μm (highest compressive stress of about -289MPa). In the same position (at depth of 50 μm), the residual stress in the as-received, untreated sample was found to be 64MPa in tension which shows that the laser shock treatment has applied a significant amount of compression at respective position within the sub-surface of the ceramic.



(a)



(b)

Figure 3. Distribution of residual stress obtained by incremental hole drilling, through the thickness of 1 layer, 2 layers in (a) and 4 and 6 layers (applied at 1J, 4.5mm spot size, 1Hz, 10ns and 1030nm) of the as-received surface in (b) of Si_3N_4 ceramics.

3.2 Surface Roughness

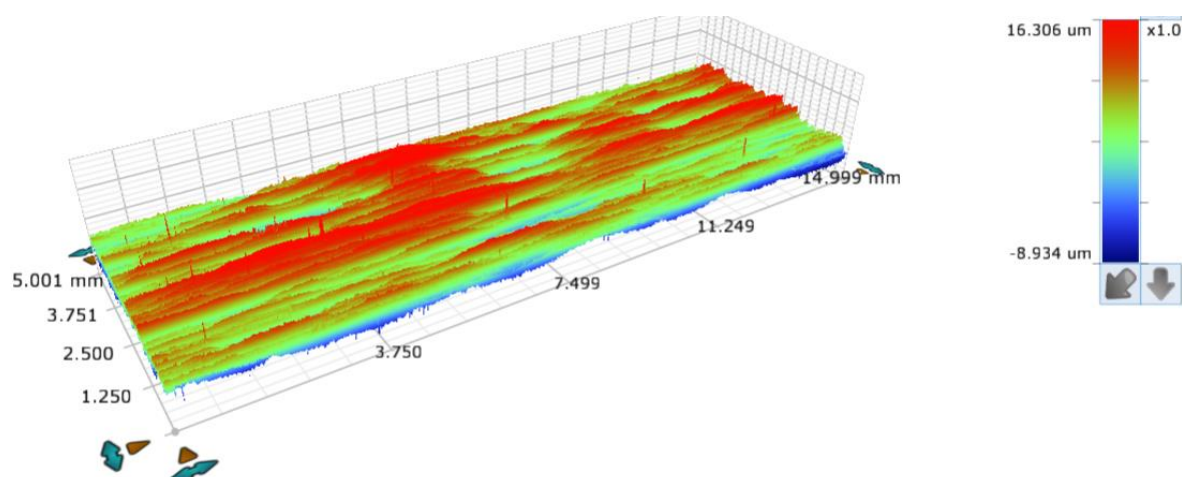
Table 3 shows various surface topography measured values for the Si_3N_4 ceramics, as-received and treated with various laser shock treatment conditions. This data was verified by the 3-D topographies presented in Figures 4(a) to (f). The S_a parameter of the as-received surface of the Si_3N_4 was measured at $1.12\mu\text{m}$. The roughness parameters began to alter once laser shock peening was applied with different numbers of peened layers. With 1 layer, the S_a parameter changed to $1.04\mu\text{m}$; and $1.08\mu\text{m}$ with 2 layers; $1.10\mu\text{m}$ with 4 layers, then $1.18\mu\text{m}$ with 6 layers. After observing the surface roughness values, it was understood that the first pulse produced to a smoother surface than the as-received surface, the S_a values then began to increase gradually as additional layers were applied. The surface started becoming rougher, beyond the roughness of the as-received surface. When we observed the surface under both the optical microscopy and the SEM, it was also evident that the surface integrity post laser shock treatment was significantly altered as seen from Figures 5(a) and (b). Previous work

that focused on topographies as result of laser shock strengthening, have shown a similar trend in both Al_2O_3 and SiC ceramics [36, 37], the onset of the laser pulse has produced a rougher surface due to the material being ablated and likewise, laser shock treatment of metallic materials has also shown increased roughness herein.

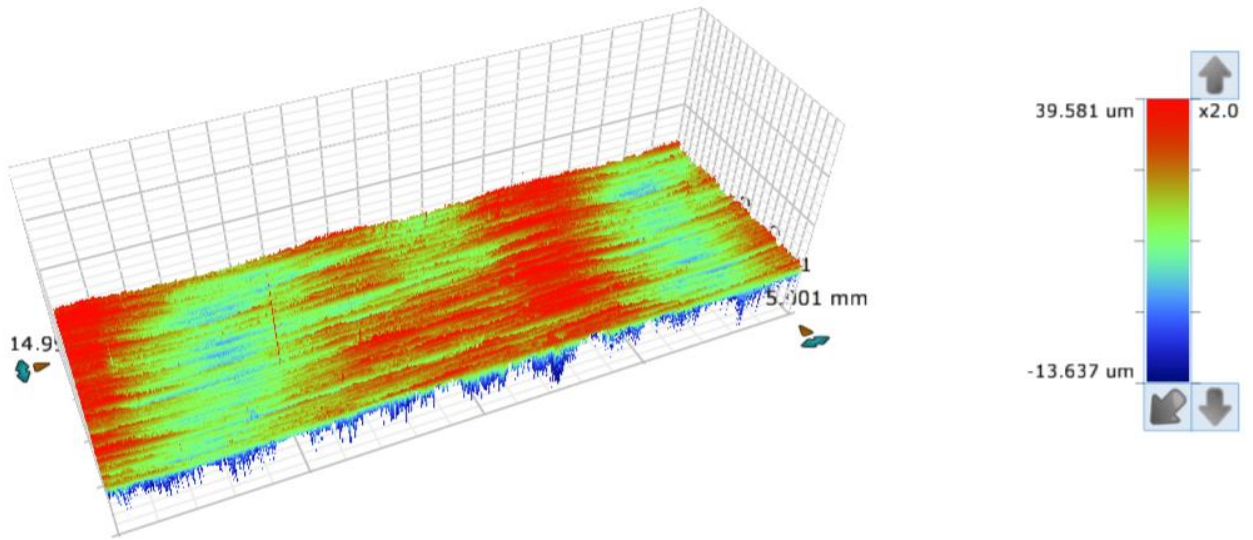
Table 3. Surface roughness of the Si_3N_4 prior-to and post laser shock treatment.

Surface Condition	Surface Roughness / μm				
	Sa	Sp	Sq	Sz	Sv
As-received	1.12	16.30	1.42	25.24	-8.93
1 layer @1J	1.04	39.58	1.29	53.21	-13.63
2 layers @ 1J	1.08	80.98	1.35	163.76	- 82.78
4 layers @ 1J	1.10	29.25	1.37	46.18	-16.92
6 layers @ 1J	1.18	72.52	1.51	13.90	- 66.55

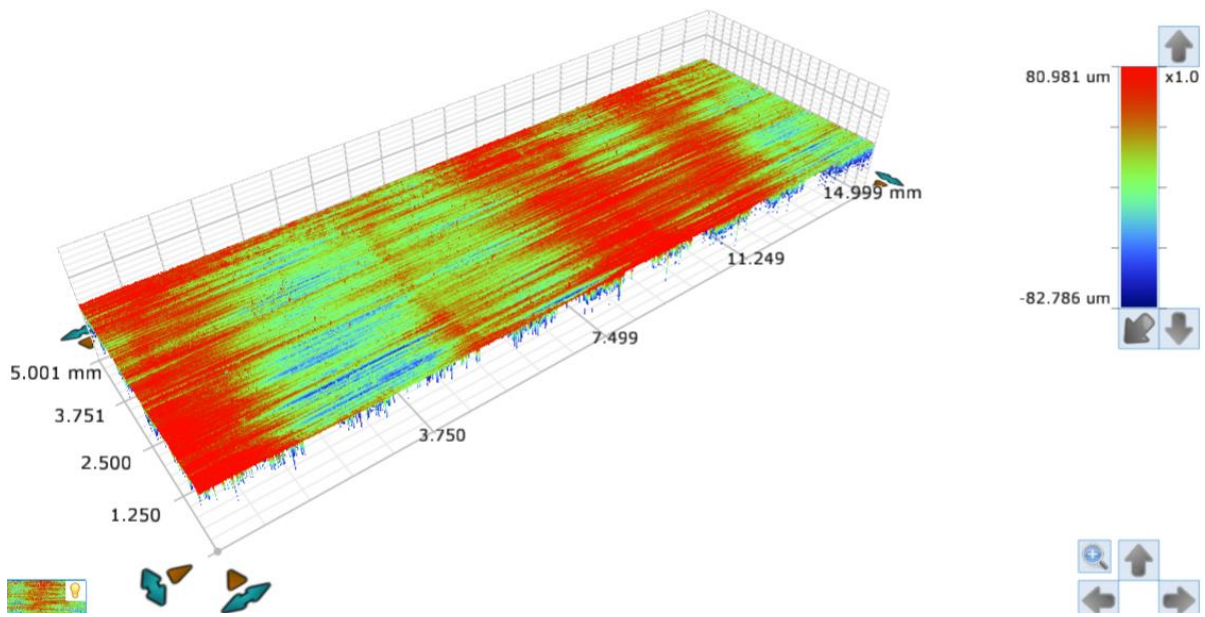
Sa = Average height of selected area; Sq = Root-Mean-Square height of selected area; Sp = Maximum peak height of selected area; Sv = Maximum valley depth of selected area; Sz = Maximum height of selected area;



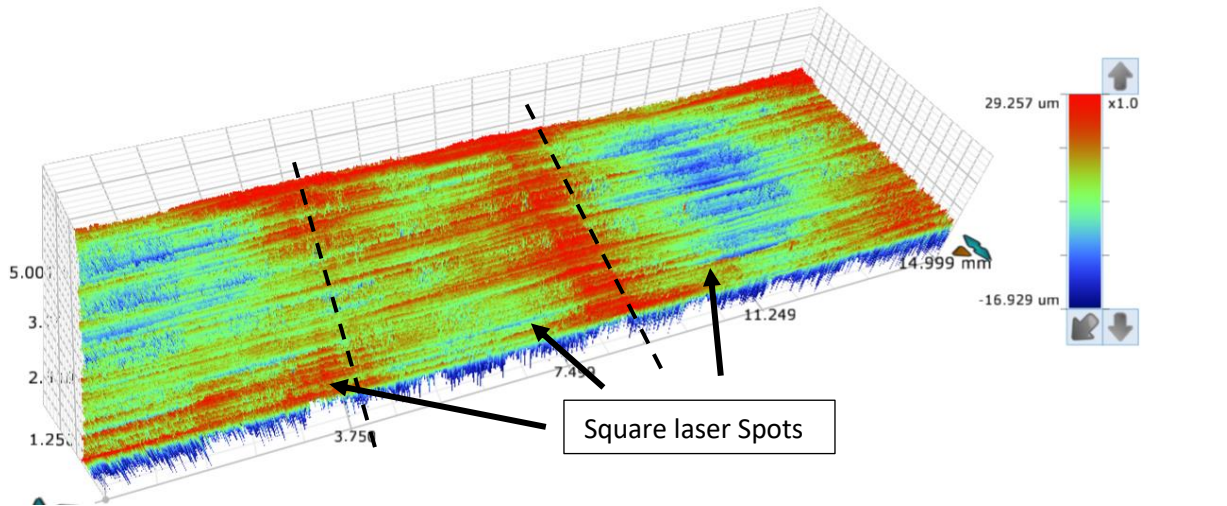
(a)



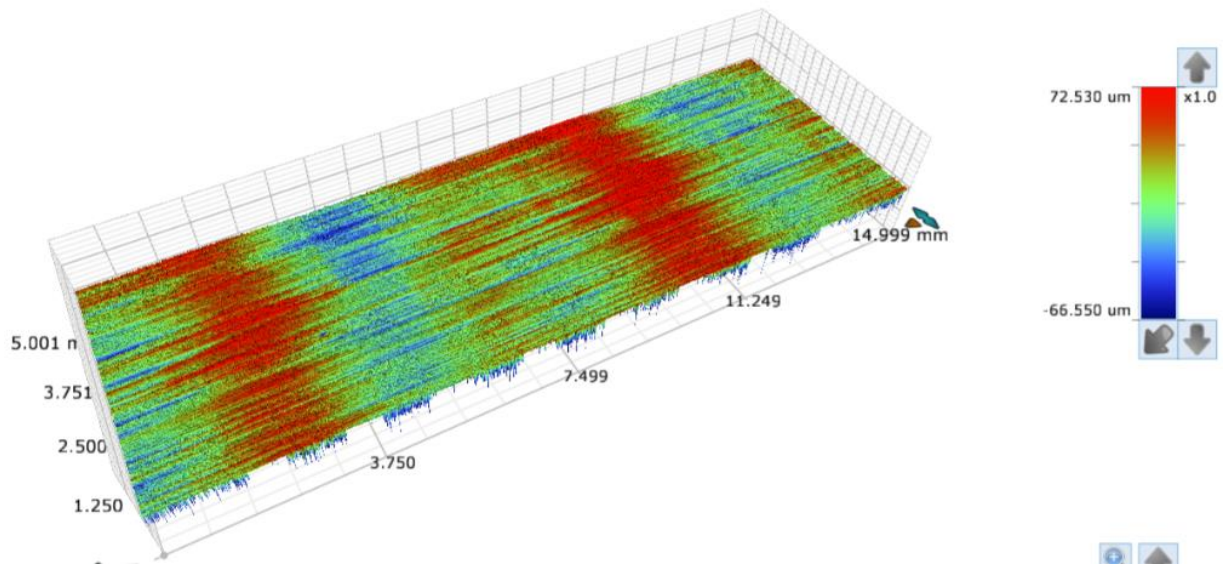
(b)



(c)



(d)



(e)

Figure 4. Illustrations of the as-received in (a) with S_a of $1.12\mu\text{m}$; 1 layer, 1J in (b) with S_a of $1.04\mu\text{m}$; 2 layers, 1J in (c) with S_a of $1.08\mu\text{m}$; 4 layers 1J in (d) and with S_a of $1.10\mu\text{m}$; 6 layers 1J in (e) with S_a of $1.18\mu\text{m}$.

3.3 Macrostructure Observations

One of the most important features when laser shock peening ceramics is to first inspect and observe any potential micro-cracks that are generated on the surface from the “instant” thermal shock sourced local thermal expansion and the exerted pressure shock-waves on the

brittle and stiff ceramic surface. Figures 5(a) to 5(e) illustrate microscopic optical images of the Si_3N_4 surface.

It is evident that striations are present. The striations seen are a result of the finishing (milling) process applied post CIPing. The existence of induced surface micro cracks is a good indication that the material has surpassed the threshold for the onset of brittle micro-cracking.

A macroscopic evaluation at 1J (1 layer), in figure 5b showed removal of both the ink layer and the effect of the square spot. Within the square spot there are few micro-cold spots evidenced, but, with additional layers applied (2 layers, 1J) the effect becomes more apparent, within the laser shock peened region, it is important to see if there is any potential cracking present. As further layers are applied (4 layers, and 6 layers) the shock treated ceramic begins to change colour with the micro-cold spots disappearing and laser impact zone becomes more fully convergent. Applying 1 layer at 4J has slightly different effect as evidenced from the difference in colour (see figure 1c). Still no evidence of a cracked surface can be seen. In all cases the effect of oxidation was observed. This oxidation was created by the methodology of shock treatment itself, not being directly similar to the typical laser shock peening process (in terms of peening with multiple layers). Specifically, after applying the very first layer the, absorptive ink layer was removed.

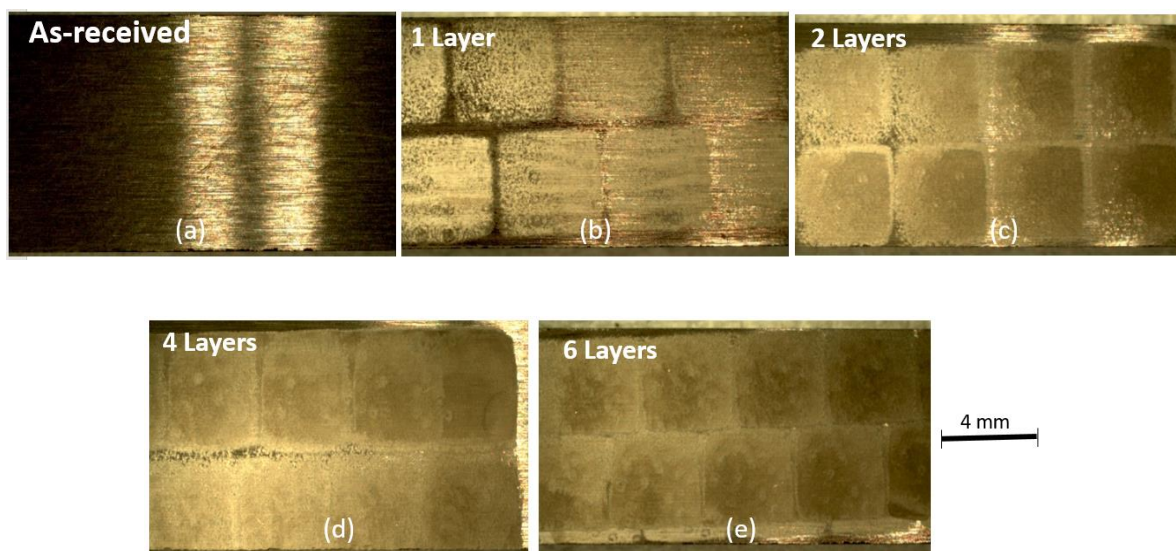


Figure 5. Illustrating the macro-structure with crack-free surface treatment evident from (a) to (e).

3.4 Surface Topography *via SEM*

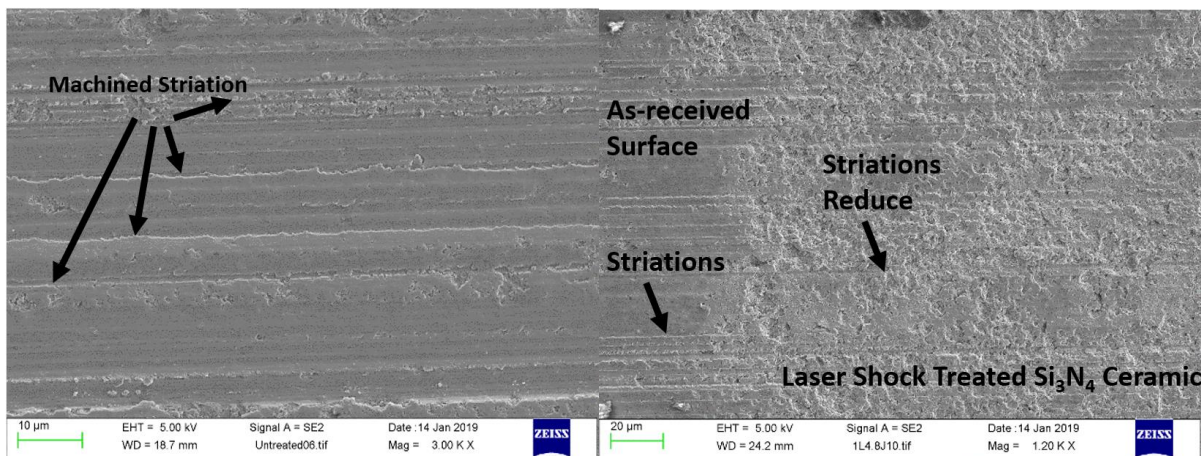
The as-received surface in Figure 6a (SEM image) shows striations from the machined surface post cold isostatic pressing (CIPing). After applying the first layer of laser shock treatment, the surface profile is altered as the machining striations were removed as shown in Figure 6b (1 layer laser shock peened sample). This is also confirmed via interpretation of the EDS spectra later in the paper (Section 3.8) showing Si₃N₄ ceramic treated with 1 layer having the striations marks from machining have been completely removed with a new composition layer being formed. This is evidenced on all the surfaces laser shock treated samples with 2 layers, 4 layers, and 6 layers of peening applied. What is also encouraging is that no cracking was found from these surfaces from laser shock treatment which otherwise defeats the objective of such a process that is undertaken for enhancing the strength and mechanical properties. With increasing the number of layers, the effect of the new surface created is more distinct. The new surface was rather evident from the optical images (shown in figure 5) and is an indication of oxidation effect taking place from the nature of the shock treatment. This type of effect was previously evidenced in previous work, whereby, a Si₃N₄ ceramic surface exposed to fibre laser was oxidised, however, there was considerably higher temperature laser-material interaction present in that case [52]. The postulation of oxidation via hydrolysis was partly due to the fact that the method of the laser shock treatment used herein is not typical to that of conventional laser shock peening.

As the number of peened layers increases, the surface becomes reconfigured with the appearance of a new layer. When applying multiple layers of laser shock treatment, the typical effect of laser shock peening has been removed because once a layer is applied the typical practice of adding new a tape or an ablative coating means the surface is protected from any other potential effects (such as compositional changes). However, in this process, we have deployed a black-ink coating as an ablative/absorptive layer only prior to

the first treatment layer. This black ink coating is removed after the first impact (layer 1).

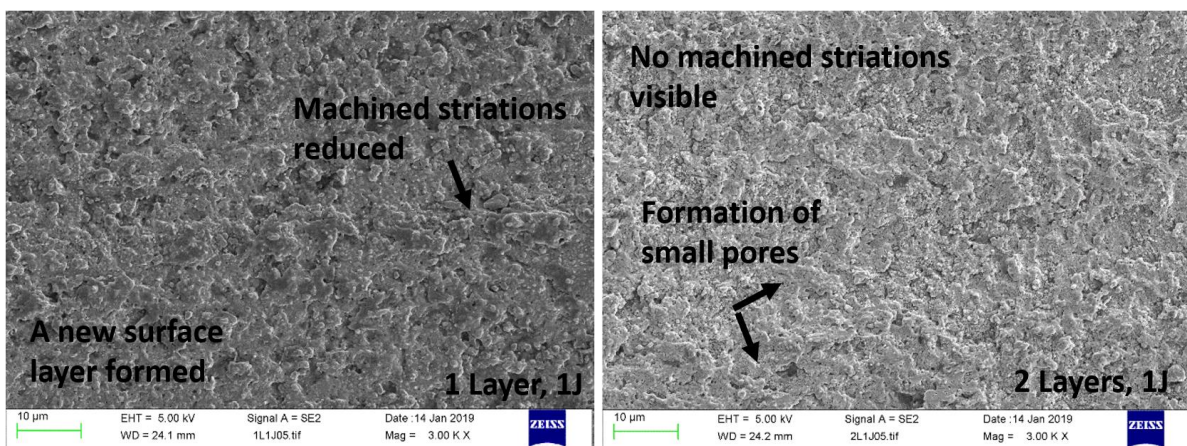
Then layer 2, 4 and 6 are applied and what this does to the Si_3N_4 is to produce an oxide layer that is rather softened as evidenced from the hardness test results shown.

Laser shock peening is a cold process; however, the treatment here was conducted in open air with water confinement layer. In this case, there was a slight reaction of the Si_3N_4 ceramic surface causing some discolouration. This is a minor effect but increasingly shows up with multiple layers applied (1J). The generation of SiO_2 was observed in other investigations of laser processing Si_3N_4 if the oxygen partial pressure is about 1 mm Hg, or above. The oxygen partial pressure is about 16 mm Hg at room temperature and so it is likely that an SiO_2 layer was formed. The layer of SiO_2 is a protective film at the Si_3N_4 surface. This occurrence of this phenomenon is sometimes it is known as passive oxidation [4].



(a)

(b)



(c)

(d)

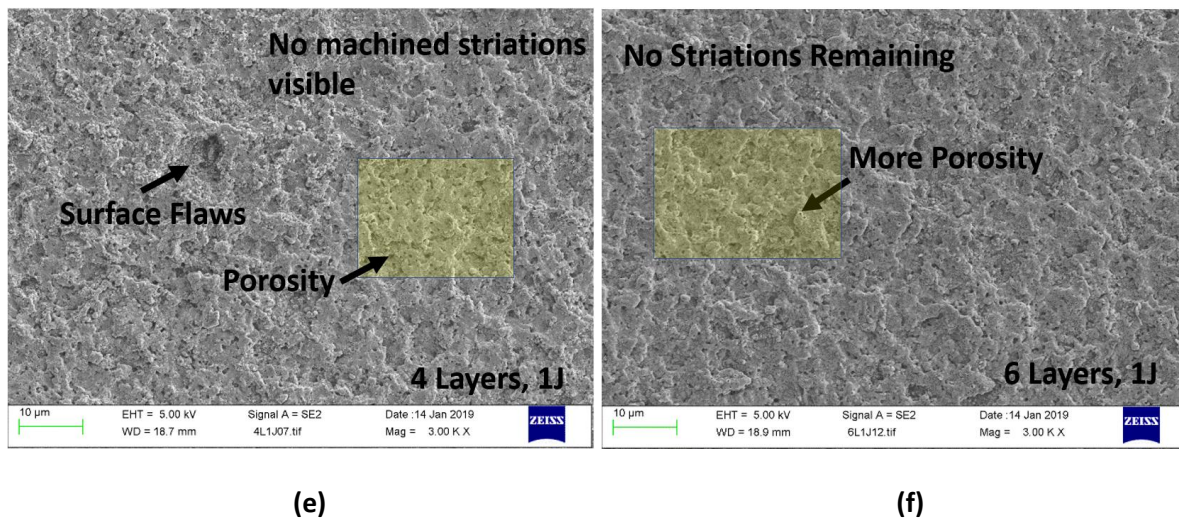


Figure 6. SEM images illustrating the as-received in (a); the interaction between the laser shock peened area and the as-received area in (b); 1 layer 1J in (c); 2 layers 1J in (d); 4 layers 1J in (e); 1J 6 layers in (f) of the laser shock treated Si_3N_4 .

3.5 Hardness Testing

Table 4 presents the hardness of laser shock treated Si_3N_4 ceramics with multiple **LSS treatment** layers. The hardness of the untreated Si_3N_4 ceramic was averaged at 1515HV. The highest hardness measured was an average of the Vickers diagonal size in both X and Y-direction and was $111\mu\text{m}$ with STDEV being $3.77\mu\text{m}$. When compared to a laser shock treated Si_3N_4 at 1J with 1 layer, the hardness was measured to be an average of 1576HV and the lowest being 1529HV. The STDEV was 49HV and was the second lowest from all the conditions measured. The average size of the diagonal indentation was $108\mu\text{m}$ and its STDEV was $3.37\mu\text{m}$. After applying additional layer (2 layers at 1J), the hardness reduced to 1527HV. In comparison to the previous sample (1 layer, 1J), this was not significantly different, the STDEV was also being 61HV. However, the size of the diagonal was $110\mu\text{m}$ which was larger than the diamond indentation produced in the previous sample. The STDEV for this footprint was $3.61\mu\text{m}$.

As the number of layers increased to 4 at 1J, the hardness decreased to 1480HV on average, the highest value from the 10 indentations was 1566HV, whilst the smallest 1394HV.

The value of STDEV increased to 70HV, indicating changes on the surface, possibly due to the increased laser shock treatment conditions. A trend is now apparent with the hardness reducing and the size of the diagonal indentation footprint now increasing to an average of 112µm. The variation from the mean increased here to a STDEV of 4.43µm.

As the number of layers increased to 6 at 1J, the hardness reduced even further to 1435HV. The highest value measured for this was 1569HV and the lowest being 1252HV. The standard deviation in hardness from the mean being 85HV. The average size of the diagonal was 114µm. The STDEV for the diagonal size was 4.28µm. So the trend is as such that the hardness is reducing with increase in the number of layers

This trend also ties well with a trend that higher hardness produces smaller indentation footprints and lower hardness produces larger footprints as result of the Vickers indentation test. This goes to show that laser shock surface treatment was producing a pseudo-ductile surface as result of softening from the effect of oxidation, as the laser shock treatment was conducted, partly without coating from applying 2 layers to 6 layers. This effect has been completely opposite to the effect of laser shock hardening that usually occurs with metals and alloys, where the hardness usually increases with increasing number of layers. The shock-wave propagation also deepens as the number of layers are induced (is applied) which produces larger stress field into metal substrates. In the case of the treatment of the Si₃N₄ ceramic, the effect was opposite, whereby, as the shock-waves penetrated deeper (with increasing layers applied), however a softening effect was observed, albeit that the surface softening is postulated as being due to surface oxidation via hydrolysis rather than a direct result of the depth of shock wave penetration. The softening effect has been reported in a previous investigation on fibre laser surface treatment of Si₃N₄ using a continuous wave laser beam [54]. It was reported that the softening took place from an oxidation effect, however, the temperature during fibre laser interactions in that case were much higher (excess of 1900°C).

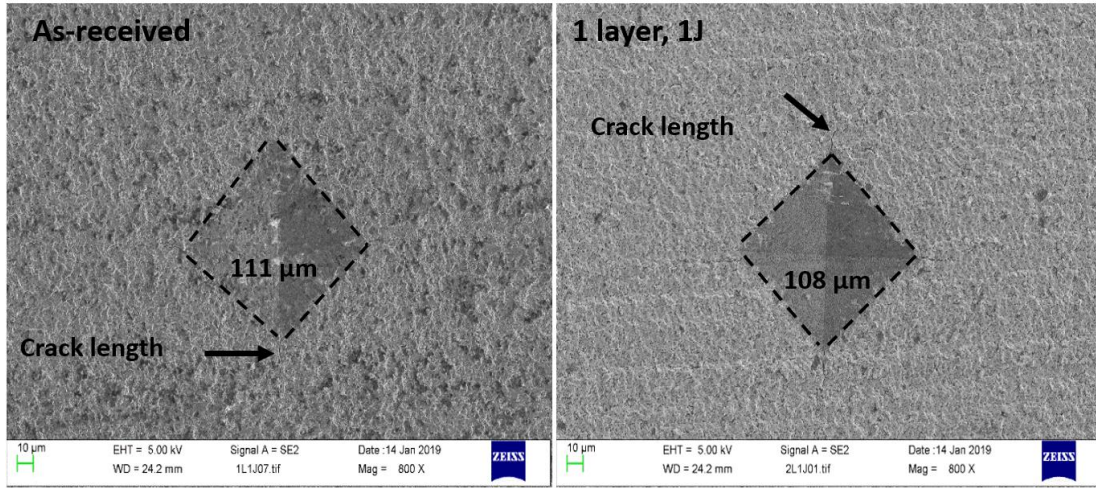
The data obtained from the hardness tests are (is deemed) reliable because the measurements were taken 10 times on each laser shock treated and as-received sample and the standard deviation suggested that the values did not fluctuate drastically. Moreover, the

surface was consistently responding well to each diamond indentation test (footprint). Therefore, the values were repeatable across all the samples measured over 10 identical indentations on one surface and then collectively all the surfaces evaluated.

Surface roughness values can influence the hardness of materials being tested in general. Having said that, one can measure the micro-hardness even on very rough surfaces. For example, micro-hardness on the worn surface subject to abrasive wear was measured in an investigation on abrasive wear resistance of high-carbon low-alloy steels [55]. The surface of ceramics can contain micro-pores and micro-cracking however, the dimension of the indentation should be much larger than the asperities on the surface. In our case, the asperities (average surface roughness over a selected area - S_a), was significantly smaller than the width of the diagonal from the diamond indentation. The highest S_a value was $1.18\mu\text{m}$, for the laser shock treated zone, whereas, the smallest average of the diagonal indentation was $108\mu\text{m}$. This was a strong indication that the surface conditions were had negligible influence during hardness testing of both the as-received and laser shock treated surfaces of the Si_3N_4 .

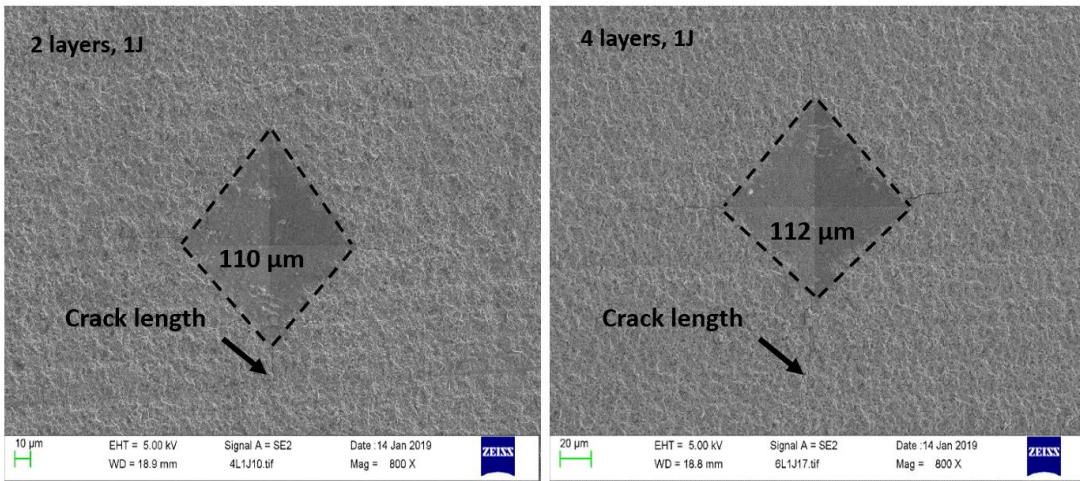
Table 4. Hardness of laser shock treated Si_3N_4 ceramics with multiple layers.

Surface Type	Average Hardness (HV)	% Change form as received	Standard Deviation (STDEV) in HV	Average Size of Diamond Indentation (μm)	Standard Deviation (STDEV) in (μm)
1 Layer, 1J	1576	1	49	108	3.37
2 Layers, 1J	1527	2	61	110	3.61
4 Layers, 1J	1480	4	70	112	4.43
6 Layers, 1J	1435	6	85	114	4.28
As-received	1515	0	45	111	3.77



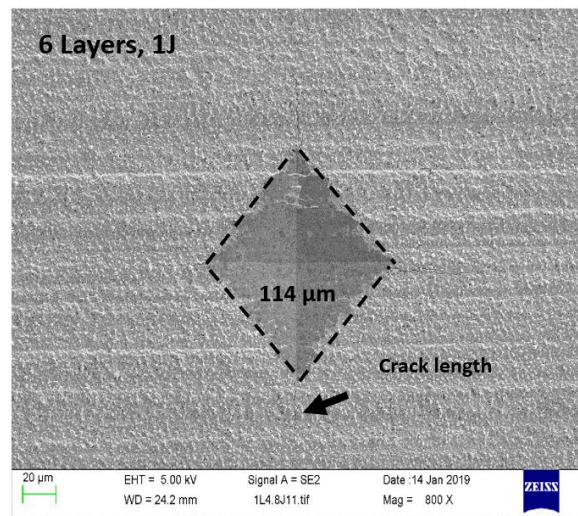
(a)

(b)



(c)

(d)



(e)

Figure 7. Example scanning electron microscopy images of the diamond footprints showing the average indentation size and associated surface cracking, on the Si_3N_4 of the as-received surface in (a), laser shock treated Si_3N_4 surface with 1 layer in (b) 2 layers in (c); 4 layers in (d), and 6 layers in (e).

3.6 Crack Length

Figure 8 illustrates the crack lengths produced as a result of the Vickers indentation on both the laser shock treated surfaces and the as-received surface of the Si_3N_4 samples. The crack lengths (flaw sizes) were measured to be an average of $197\mu\text{m}$ for the as-received sample. As more laser shock treatments were applied, it reduced these to $158\mu\text{m}$ at 1 layer, then $144\mu\text{m}$ at 2 layers, then rose to $170\mu\text{m}$ at 4 layers and $181\mu\text{m}$ with 6 layers. As number of layers increases hardness drops- most likely due to the oxidation-hydrolysis effect postulated, smallest crack lengths being generated from the 2 layer applied condition, inferring an optimum LSS condition for lowest flaw size and consequent higher K_{1c} .

This was attributed to the fact that a compressive residual stress of higher magnitude was present on those samples. The crack length standard deviation was $12\mu\text{m}$ for the as-received surface, whereas, the STDEV reduced to $9\mu\text{m}$ for 1 layer, then $11\mu\text{m}$ for 2 layers, indicating that the surface became increasingly regular from the laser shock treatment and resulted to more consistent crack geometry during Vickers indentation.

As laser shock treated layers increased to 4 and 6, the STDEV also increased to $16\mu\text{m}$ and $24\mu\text{m}$ respectively. This was attributed to the thickening of the oxide layer produced firstly creating an uneven surface that regulated the cracking geometry. Figure 9 shows illustration of Vickers indentation footprints at higher resolution for the as-received condition, 1 layer and 6 layers (1J) treatments. The crack tips for the respective surfaces do not see (illustrate) a significant change (difference) except all being characteristic of brittle fractures (crack propagation), thus, only selected images were demonstrated.

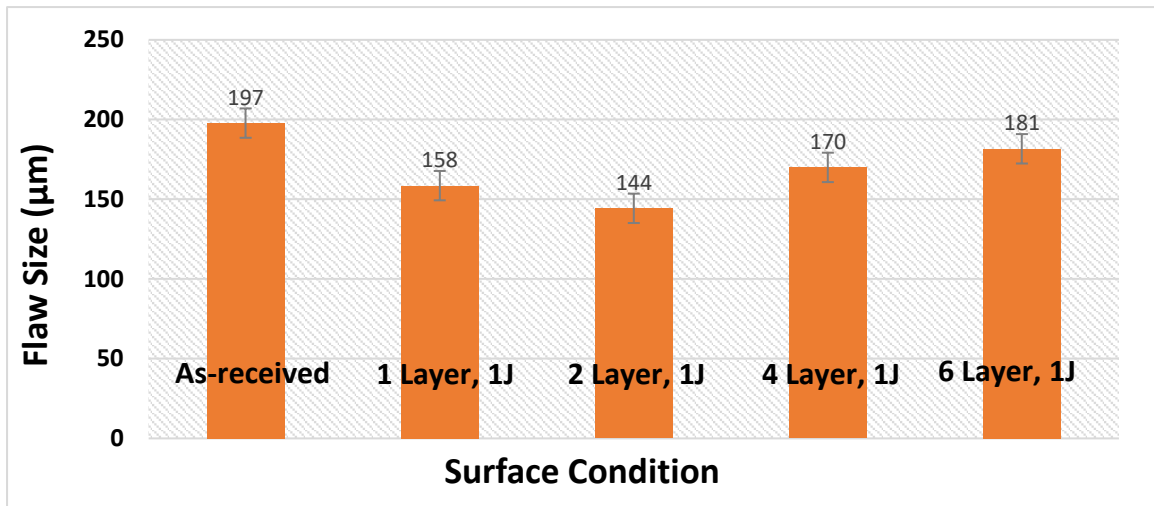
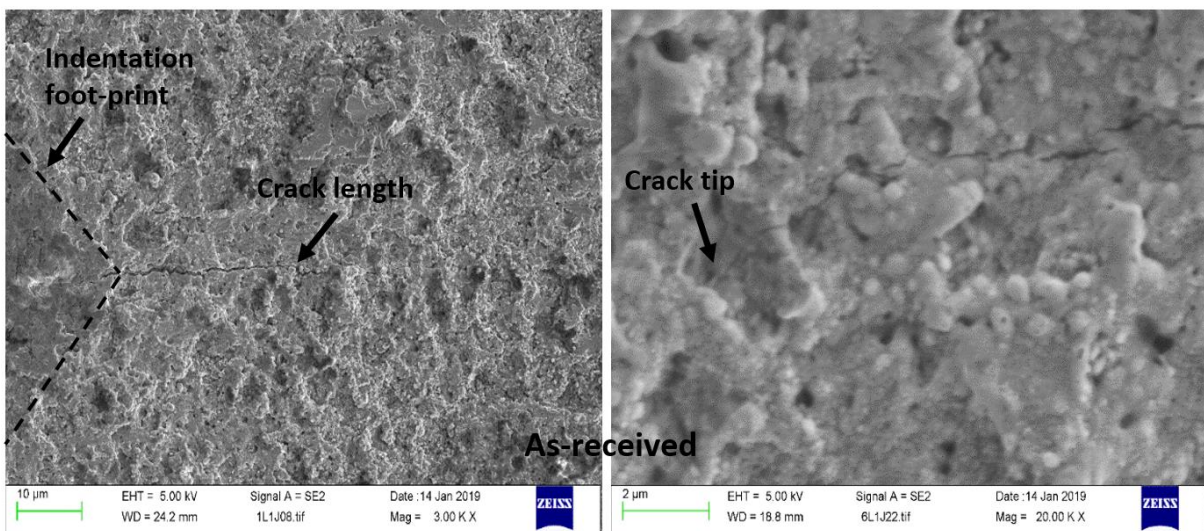
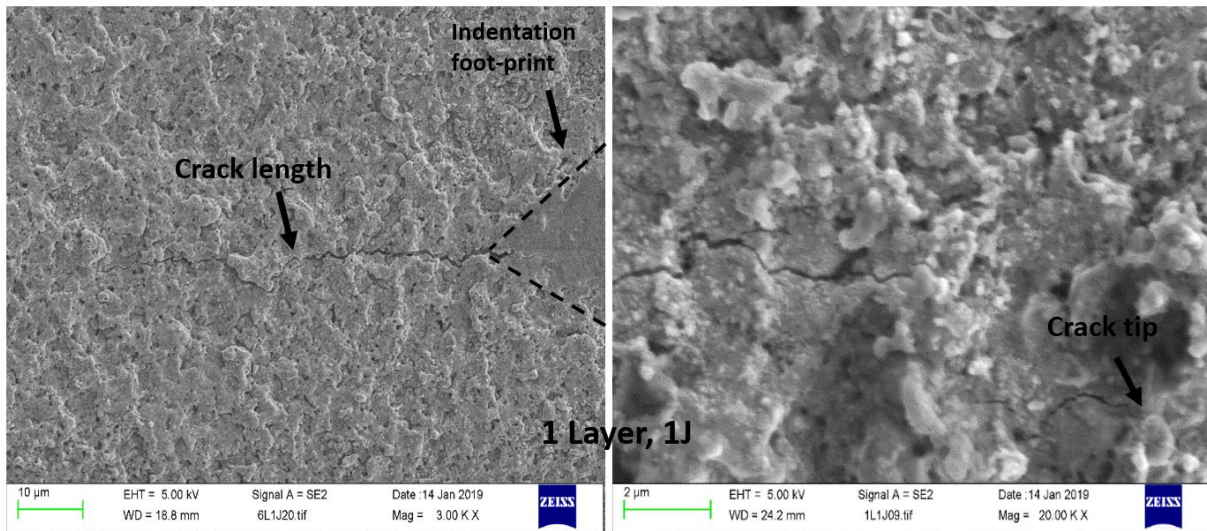


Figure 8. illustrating the average crack lengths (flaw size) from a Vickers indentation of the as-received and laser shock strengthened Si_3N_4 ceramic.



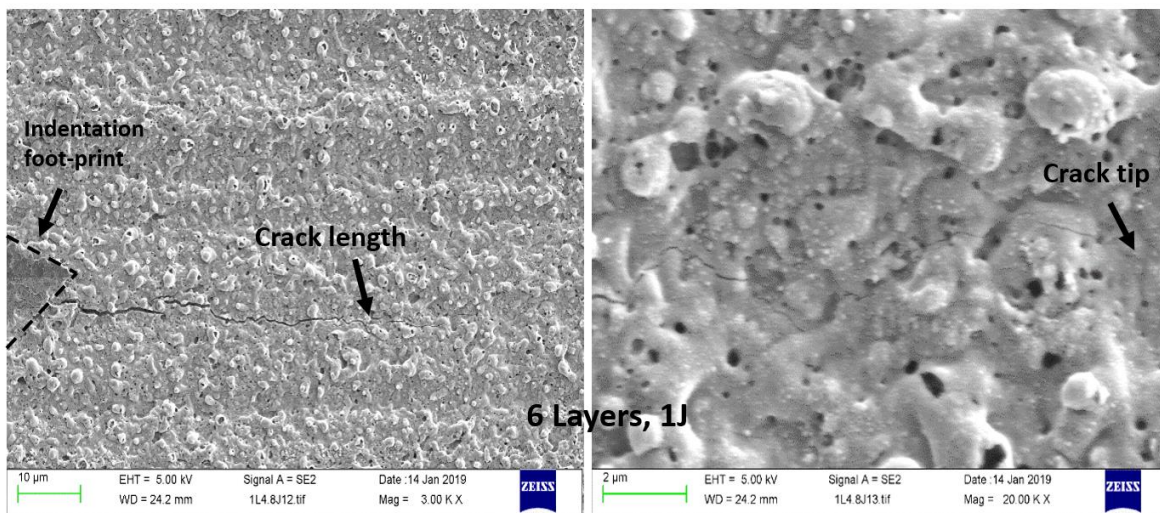
(a)

(b)



(c)

(d)



(e)

(f)

Figure 9. Illustration of indentation crack lengths at high resolution for as-received surface in (a) and (b); (c) 1 layer, 1J, and (d) and 6 layers, 1J (e) and (f).

3.7 Surface Fracture Toughness (K_{IC})

Figure 10 represents surface K_{IC} value of the as-received and laser shock treated Si_3N_4 as calculated via the Vickers indentation method (equation 3). Firstly, it was evident that all surfaces treated with laser shock treatment technique resulted to a higher K_{IC} , compared to the as-received surfaces. The average K_{IC} measured for the as-received surface over 10

valid indentations was 2.89 MPa.m^{1/2} after applying 1 layer, the average K_{IC} was 3.96 MPa.m^{1/2} and further increased to 4.63 MPa.m^{1/2} when 2 layers were applied. This was the highest K_{IC} measured from all the conditions tested and an increase of 60% when compared to the as-received surface. When 4 layers were applied with 1J, the K_{IC} reduced to 3.68MPa.m^{1/2}.

After increasing the number of layers to 6, with 1J applied, the K_{IC} was 3.39 MPa.m^{1/2}. This was the lowest K_{IC} value measured, from all the laser shock treated conditions applied. The K_{IC} fluctuated because of the change in the crack length found for each of the samples for example the crack length was the lowest, the sample shock treated with 2 layers surface condition and rendered the highest K_{IC}. The crack length in general is a big contributor in the K_{IC} calculation. If the crack length increases, K_{IC} naturally decreases as the ceramic indicates, loss of strength (loss of resistance to applied force), thus, creating larger cracks during indentation response. In addition, the residual stress found on the surface with lowest crack was high in compression (-289MPa at 48µm for the 2 layer 1J condition as shown in figure 3a). The residual stress can be attributed to local surface dislocation activity within the Si₃N₄ [54]. In summary shortest crack lengths from the Vickers indentation test correspond to the highest compressive residual stress induced from the 2 layer, 1J treatment

It was also evident from the optical images that there was some decolouration post laser shock treatment. This is attributed to increase in oxygen content at the surface, thus, EDS, analysis was performed to check for this effect. This oxide layer was thickening with increase in the number of laser shocks treatment layers applied. This ultimately, resulted to softer surface that also contributed to the increase in K_{IC}.

It must be noted that the standard deviation for the laser shock treated sample K_{IC} results (Figure 10) were similar to the as-received surface for the surfaces treated with 1 layer, 2 layers and 4 layers. However, for 6 layers the STDEV was double which indicated that the surface K_{IC} fluctuated considerably due to the thick oxide layer observed.

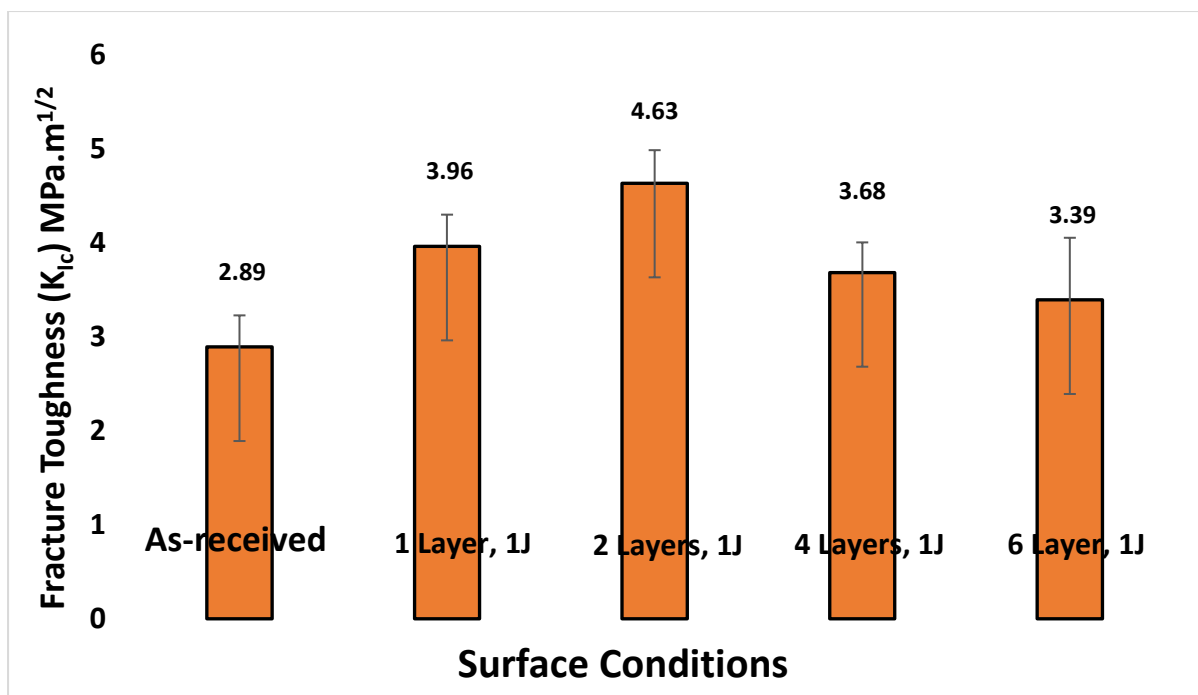


Figure 10. K_{1c} of the as-received and laser shock strengthened Si_3N_4 ceramic.

3.8 Elemental Analysis

Figure 11 shows elemental data of both the as-received and the surface treated with 2 layers which comprised of the highest compressive stress and highest K_{1c} from all of the samples. It is postulated that the discolouration evident in the optical images was as result of oxidation and was a contributory factor in influencing the K_{1c} of the Si_3N_4 . This can now be better understood with the data obtained from EDS as a mechanism to check this. The as-received surface composition looks comparable to the manufacture's specification. Other surfaces rendered promising results as the trends match those in paper thus far. Specifically comparing the two surfaces; firstly in the absence of laser shock processing (as received sample) and subsequently after laser shock processing. The Si content is identical, however, N (nitrogen) has reduced after laser shock treatment, whilst, the O content has increased from 13.2 wt% to 25.8 wt% which is an increase of 12.6 wt%. This confirmed that oxidation is taking place, which was somewhat surprising as laser shock treatment would not involve any heating and only pressure is applied rather than a thermal input. Nonetheless, it can be therefore, concluded that the increase in the surface K_{1c} after laser shock treatment was due to the fact

that the oxide layer created a surface that resisted cracking over the surface of the Si_3N_4 . This rendered reduction in crack lengths as result of the diamond indentation and thus, increased the K_{IC} of the material.

Since **conventional high temperature** oxidation occurs at **the** decomposition temperature **of** the Si_3N_4 which is about 1900°C , it is unlikely that laser shock treatment conducted in ns pulse regime has created this. We postulate that the oxidation has resulted from more of a hydrolysis process creating a chemical reaction at the surface level of the Si_3N_4 ceramic during exposure to water + plasma/photons **and associated LLS generated shock waves**. **The process of hydrolysis can be induced by this**, whereby, photons and the plasma generated retained in water confinement have created bond breakage where, nitrogen is lost **from the Si_3N_4 surface** to form silicon oxide or SiO_2 .

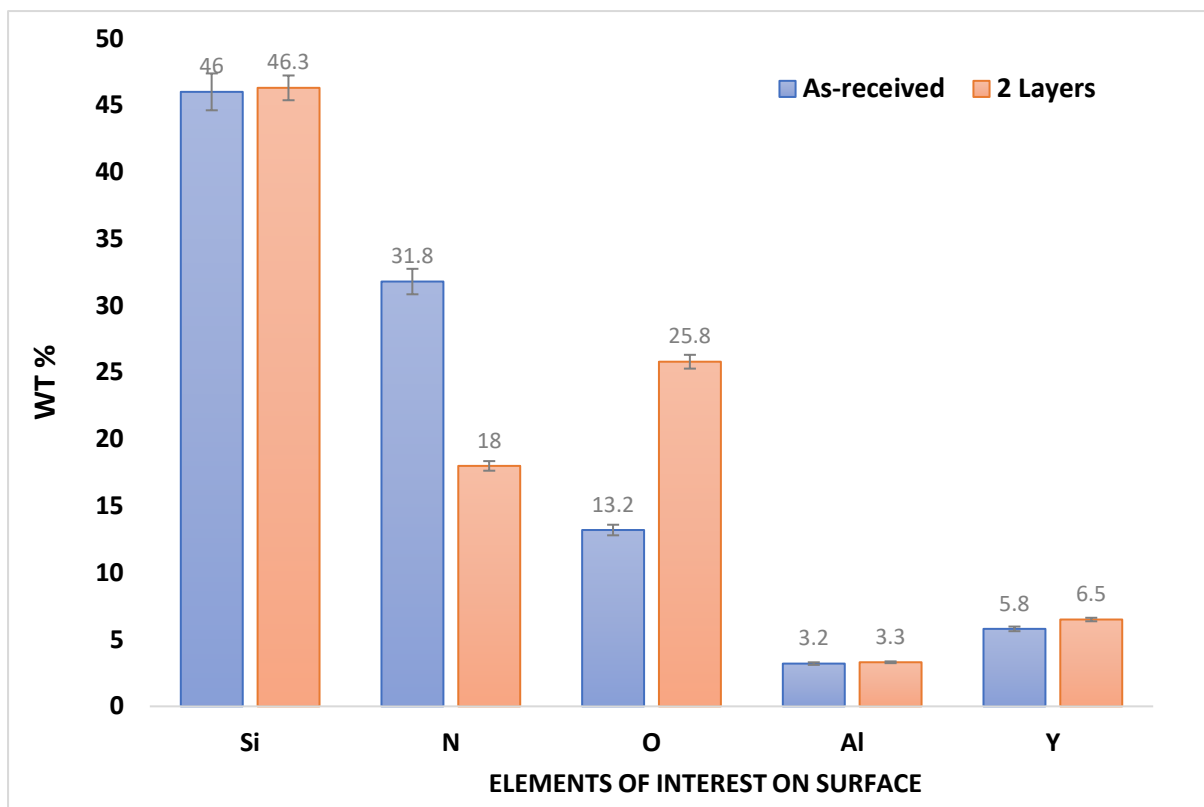


Figure 11. Elemental data obtained from the EDS spectra showing surface of the Si_3N_4 before and after laser shock treatment (2 layers).

Figure 12 shows SEM micrographs of the cross-section of both the laser peened area with 2 layers and the untreated (as-received) area. The sample treated with two layers was selected because it comprised of the highest compressive residual stress and oxygen content. The voids, cracking, and particle size appeared to be comparable in both samples and the light grey area is likely to be a catalyst, whilst the dark grey areas are grains of the Si_3N_4 matrix.

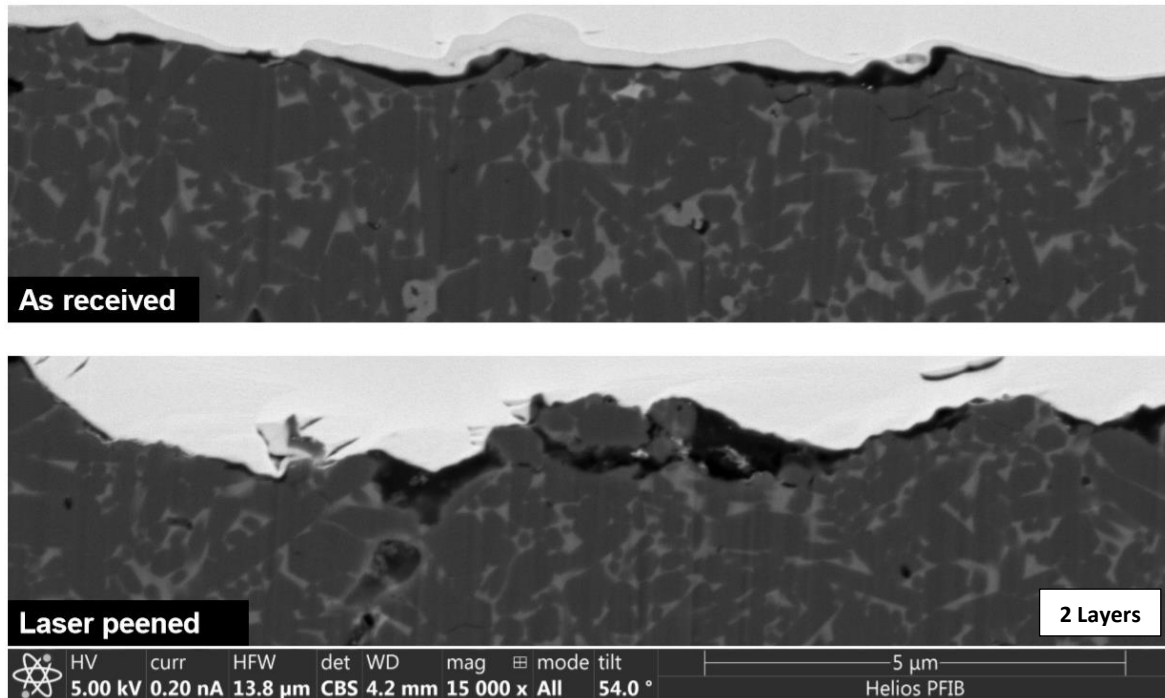


Figure 12. Cross-sectional micrograph of both the laser shock peened area with 2 layers and the untreated (as-received) area of the Si_3N_4 .

From the cross-sectional EDS results in Figure 13, it was found that there were no obvious differences; particularly, regards to oxidation. The EDS values from the two samples were essentially the same. This meant that oxidation was only found on the surface, and it would therefore have no effect on the sub-surface such as increased compressive stress which was observed particularly found on sample with 2 layers, thus the compressive stress evident would be due to the plasma-driven shock waves.

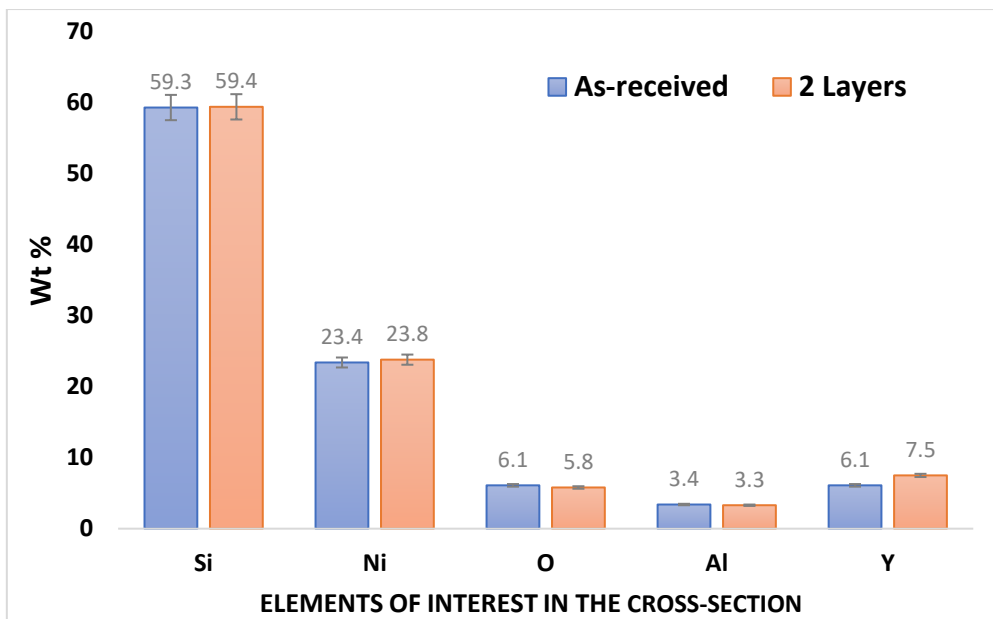
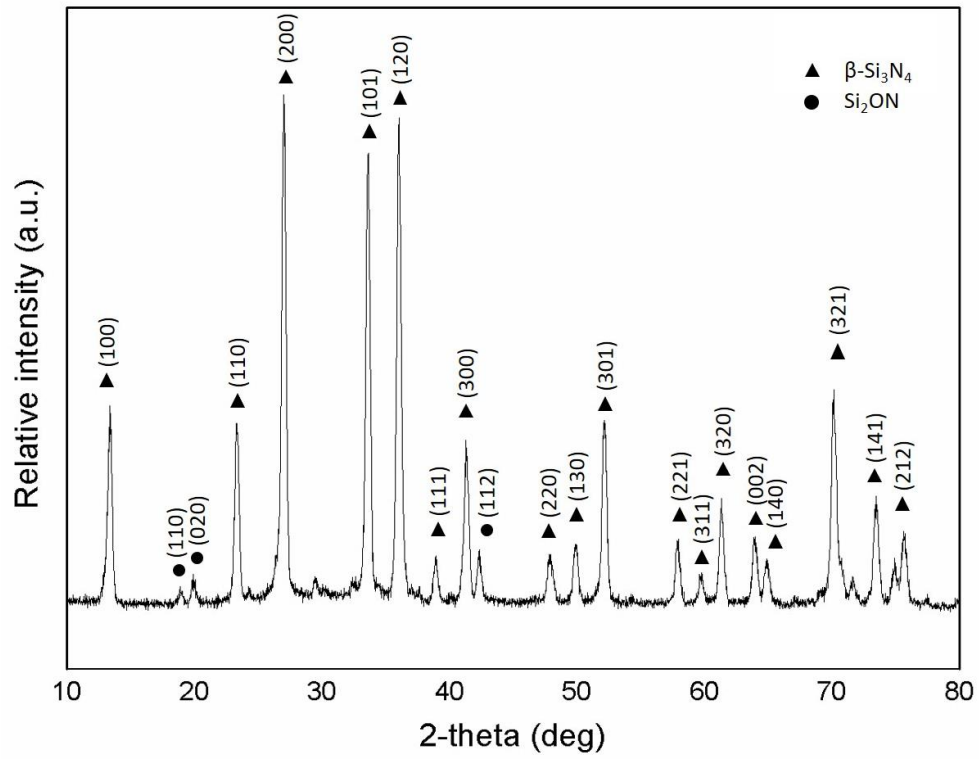


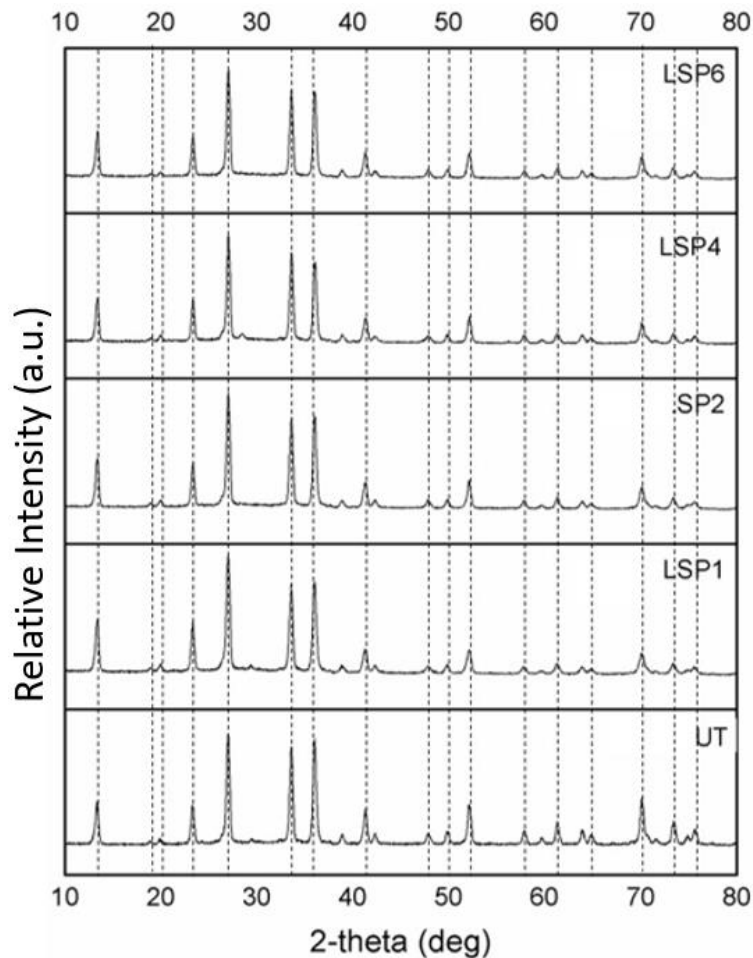
Figure 13. Illustration of elements presented in the cross-section of the as-received and laser shock treated Si_3N_4 with 2 layers from the EDS Spectra.

3.9 Phase Distribution

Phase changes often take place in metallic materials during LSP [56]. Laser shock processing of alumina ceramic was reported to **generate** no change in phase **as reported** in our previous publication [37]. Since the effects of laser shock peening of Si_3N_4 ceramic have not previously been explored, it would add to our understanding if any phase changes result from the process. However, the laser shock peening does not alter the phases. The phases were found to be Beta Si_3N_4 (Card No. 04-004-6608) and Si_2ON (silicon oxide nitride; Card No. 00-009-0246). The **X-ray diffraction** data in Figure 14 shown no change in peaks between the laser shock strengthened surface and untreated surface. The microstructural evaluation suggests that no changes in the phase beyond the sub-surface of the laser shock treated Si_3N_4 except the oxidation already found on the surface as previously discussed.



(a)



(b)

Figure 14. X-Ray diffraction patterns of the phase analysis of the as-received (UT (untreated)) surface in (a) and (b) the as-received (UT) and laser shock strengthened samples.

3.10 Laser Material Interaction

Table 5 shows the overview of results of hardness, indentation size, crack length, K_{IC} residual stress and the magnitude of residual stress (highest), with respect to depth for all the laser shock treatment conditions applied to the Si_3N_4 ceramic. During laser shock treatment of the Si_3N_4 ceramic, a series of events takes place (see Figure 15). Firstly, it should be noted that with the black-ink layer applied as the ablative coating, the ceramic was being oxidised as more energy was being applied. This layer thickened as more laser peening layers were being added. This is evident simply from the optical images in Figure 5. When multiple, laser pulses

are applied to the Si₃N₄ ceramic, the first layer interacts with the laser pulses and becomes removed. At the same time, the standard chain of events that occur with laser shock peening process tend to occur, whereby, the plasma plume generates shock pulse pressure that travels into the surface and the sub-surface. It is believed that with the presence of water confinement layer (that constrains plasma expansion such that it only generates shock waves into the substrate) and the laser material interaction temperature is less than the melting temperature of the Si₃N₄. The 10ns pulse duration applied herein, is not long enough for Si₃N₄ to reach decomposition temperature and begin to melt (1900°C).

Table 5. Material response for all the laser shock treated conditions applied to the Si₃N₄ ceramic.

Surface Conditions	Indentation Size (µm)	Crack Length (µm)	Hardness (HV)	Fracture Toughness (MPa)	Residual Stress (MPa) Peak Compressive Stress
As-received	111	198	1515	2.83	-154@16µm
1 Layer, 1J, 4.5mm Ø	108	159	1576	3.96	-126 @ 80µm
2 Layers, 1J, 4.5mm Ø	118	144	1527	4.63	-290@50µm
4 layers 1J, 4.5 mm Ø	112	170	1480	3.68	-89@160µm
6 Layers, 1J, 4.5 mm Ø	114	182	1435	3.39	-49 @ 160 µm

For the samples treated with 1 and 2 layers; what tends to happen is that the cracks are being arrested post laser shock treatment and deflected away by compressive residual stress measured for both of these samples. This in turn, led to increased K_{Ic} and lower crack lengths generated during Vickers indentation tests.

As the 4th and 6th layer was applied, the laser-material interaction increased – thickening the oxidation effect (oxide layer) as seen from the SEM and the optical images. This was attributed to hydrolysis during the laser-material interaction. With increased oxide layer, there tends to be a compositional modification, leading to lower crack length via softer

surface layer created after surface shock treatment leading to higher K_{Ic} . There appears to be an optimum laser condition (2 layers at 1J) for highest compressive residual stress and surface K_{Ic}

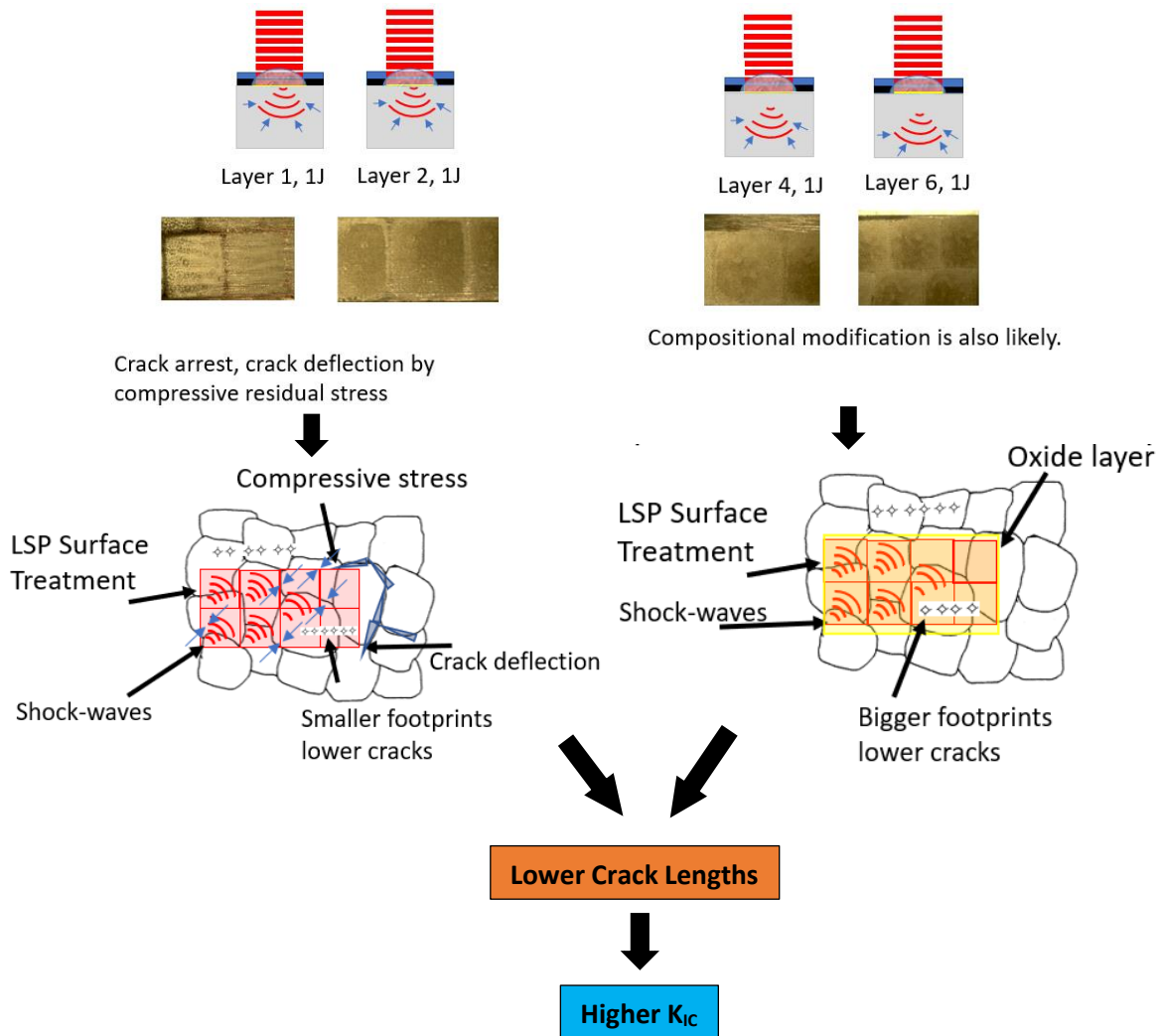


Figure 15. A schematic representing the effects of Si_3N_4 being treated with 1, 2, 4, and 6 layer at 1J, and 4mm spot diameter as well as a graphical illustration of the laser shock treatment effects, used herein resulting into differing material response, such as crack deflection, with compressive stress generation with layer 1 and 2 layer(s) applied, and the oxide layer with samples treated by 4 and 6 layers.

4.0 Conclusions

A comprehensive study was conducted for the first-time on a Si_3N_4 ceramic using a state-of-the-art DiPOLE laser to undertake laser shock treatment of (LST) with a square shape beam. This work is significant because this is a first-step in understanding the laser shock treatment response of ceramics and forms a foundation in performing beneficial laser shock treatment of Si_3N_4 ceramics in future research. This also opens new avenues where ceramics currently fail due to lack of toughness and inability to generate plasticity **to retard crack propagation**. The work elucidates the effects of multiple layer surface treatment. Specific conclusions made are:

- A crack-free laser shock treatment of a brittle Si_3N_4 ceramic was produced.
- The best parameters that rendered the highest compressive stress were $0.62 \text{ GW}/\text{cm}^2$ at 2 layers followed by 1 layer at 1J, 4.5mm spot, 10ns, and 1054nm.
- Incremental hole drilling results showed the highest compressive stress of -289 MPa at a depth of $50\mu\text{m}$ with 2 layers, followed by -126 MPa at $80\mu\text{m}$ with 1 layer, -89 MPa at $160\mu\text{m}$ and -49 MPa at $160\mu\text{m}$ for 4 and 6 layers. This was verified by comparing the as-received samples, which comprised of **a tensile residual stress of 64MPa** at $48\mu\text{m}$ depth and a peak tensile stress of 160 MPa at a depth of $112\mu\text{m}$.
- The highest surface fracture toughness (K_{IC}) was enhanced over 60% with 2 layers **of laser surface treatment**, whilst, the K_{IC} for other laser shock treated surfaces were also enhanced considerably.
- The roughness was $1.12\mu\text{m}$ for the as-received surface and reduced to $1.04\mu\text{m}$ with 1 layer, $1.08\mu\text{m}$ with 2 layers, $1.10\mu\text{m}$ with 4 layers and $1.18\mu\text{m}$ for 6 layers;
- Oxidation was found on the surface through hydrolysis - chemically, changing the only top layer ($5\mu\text{m}$) of the Si_3N_4 ceramic to SiO_2 . Oxidation did not form within the sub-surface region, and was not evident in the cross-section.

The results herein are significant as the paper paved a way for laser shock treatment (LST) of Si₃N₄ ceramics with plasma-driven shock waves with an understanding of the laser material interactions to progress further laser peening Si₃N₄ ceramics in future research.

Acknowledgements

The leading author would like to acknowledge the laser scientist and staff as the Central Laser Facility at STFC, Harwell, for organizing the experimentation for laser shock peening, these are in particular, Jodie Smith, Saumyabrata Banerjee, and Jonathan Phillips.

5.0 Contributions

- Pratik Shukla, designed and planned the research, conducted the laser experiments and the respective investigations as well as drafted the manuscript.
- Xiaojun Shen, undertook residual stress measurements and illustrated the incremental hole-drilling data.
- Ric Allott, assisted with laser shock treatment experiments at STFC, central laser facility and provided access and time on the DiPOLE laser system.
- Klaus Ertel assisted with DiPOLE laser experiments.
- Stuart Robertson and Robert Crookes provided expertise on microstructural evaluation and EDS analysis.
- Ann Zammit contributed to obtaining the phase transformation data.
- Michael Fitzpatrick and Houzheng Wu and **Phil Swanson**, edited the manuscript and enhanced the technical quality and the overall content of the manuscript.

Funding:

The authors acknowledge use of facilities within the Loughborough Materials Characterization Centre and for access to the Helios PFIB, funded by the EPSRC grant EP/P030599/1.

6.0 Data Availability

The raw data required to reproduce these findings are available upon request to the leading author of the manuscript. The processed data required to reproduce these findings are also available upon request to the leading author of this manuscript.

7.0 References

1. C. Santos, S. Ribeiro, K. Strecker Jr., D. Rodrigues, C.R.M. Silva, Highly dense Si₃N₄ crucibles used for Al casting: An investigation of the aluminum–ceramic interface at high temperatures, *Journal of Materials. Processing and Technology*. 184 (2007) 108-114.
2. D. Pakuáa, L.A. Dobrzański, K. Goáombek, M. Pancielejko, A. KĚiř, Structure and properties of the Si₃N₄ nitride ceramics with hard wear resistant coatings, *Journal of Materials, Processing and Technology*. 157-158 (2004) 388-393.
3. S. Hampshire, Silicon nitride ceramics – review of structure, processing and properties, *Journal of Achievements in Materials and Manufacturing Engineering*. 24(1) (2007) 43 – 50.
4. D. Richardson, *Modern Ceramic Engineering*. Third Edition, published by CRC Press, Taylor & Francis Group. (2006).
5. P. Shukla, *Viability and Characterization of the Laser surface Treatment of Engineering ceramics*, A Doctoral Thesis: Loughborough University (2011) United Kingdom.
6. S. Kiani, K. Leung, V. Radmilovic, A. Minor, J-M. Yang, D. Warner, S. Kodambaka, Dislocation glide-controlled room temperature plasticity in 6H-SiC single crystals. *Acta Materialia* 80 (2014) 400-406.
7. E. Camposilvan, M. Anglada, Size and plasticity effects in zirconia micropillars compression. *Acta Materialia* 103 (2016) 882-892.
8. T. Nishimura, X. Xu, N. Hirotsaki, R. Xie, H. Tanaka, Plastic Deformation of Silicon Nitride Nano-Ceramics, *Key Engineering Materials*. 352 (2007), 189-192.
9. S. J. Dillon, M. P. Harmer, Multiple grain boundary transitions in ceramics: a case study of alumina. *Acta Materialia* 55 (2007) 5247-5254.
10. W. Li, X. Yao, P. Branicio, X. Zhang, N. Zhang, Shock-induced spall in single and nanocrystalline SiC. *Acta Materialia*. 140 (2017) 274-289.
11. I. Wei Chen, An Xue. Liang Development of Superplastic Structural Ceramics, *Journal of American Ceramic Society*. 73(9) (1990) 2585 – 2609.
12. T. Rouxel, F. Rossignol, J.L. Besson, P. Goursat, J. F. Goujaud, P. Lespade, Superplastic Deformation of a Monolithic Silicon Nitride. In: Bradt R.C., Brookes C.A., Routbort J.L. (eds) (1995) *Plastic Deformation of Ceramics*. Springer, Boston, MA.

13. J. W. Edington, K N Melton, and C. P. Cutler, "Superplasticity," *Prog. Mater. Sci.*, 21(2) (1976) 61-170.
14. F. Wakai, S. Sakaguchi, and Y. Matsuno. Superplasticity of Yttria-Stabilized Tetragonal ZrO₂ Polycrystals," *Adv. Ceram. Mater.*, 1(3) (1986), 259-63.
15. Z. F. Wakai, Y. Kodama, and T. Nagano, Superplasticity of ZrO₂ Polycrystals, *Jpn. J. Appl. Phys.*, 28 (1989) 69-79.
16. Camposilvan, E. & Anglada, M. Size and plasticity effects in zirconia micropillars compression. *Acta Materialia* 103 (2016) 882-892.
17. S. Kiani, K. Leung, V. Radmilovic, A. Minor, J-M. Yang, D. Warner, and S. Kodambaka, Dislocation glide-controlled room temperature plasticity in 6H-SiC single crystals. *Acta Materialia* 80 (2014) 400-406.
18. F. Longy, K. Cagnoux, Plasticity and microcracking in shock-loaded Alumina, *Journal of American Ceramic Society*. 76, (1989) 971 – 979.
19. H. Z. Wu, C. W. Lawrence, S. G. Roberts, B. Derby, The Strength of Al₂O₃/SiC Nanocomposites after grinding and annealing, *Acta Materialia*. 46 (11) (1998) 3839 – 3748.
20. M. Bhattacharya, S. Dalui, N. Dey, S. Bysakh, J. Ghosh and A. K. Mukhopadhyay, Low strain rate compressive failure mechanism of coarse grain alumina, *Ceramics International*. 42 (2016) 9875 – 9886.
21. H. Wu, S. G. Roberts and B. Derby, Residual stress distributions around indentations and scratches in polycrystalline Al₂O₃ and Al₂O₃/SiC nanocomposites measured using fluorescence probes, *Acta Materialia*. 56 (2008) 140 – 149.
22. H. Wu, S. G. Roberts, B. Derby, Residual stress distributions around indentations and scratches in polycrystalline Al₂O₃ and Al₂O₃/SiC nanocomposites measured using fluorescence probes, *Acta Materialia*. 56 (2008) 140 – 149.
23. M. Gerland, M. Hallouin, H. N. Presles, Comparison of two new surface treatment processes, laser-induced shock waves and primary explosive: application to fatigue behavior, *Materials Science and Engineering: A*, Volume 156 (2), (1992)175-182.
24. J. E. Masse, G. Barreau, Laser generation of stress waves in metal, *Surface and Coatings Technology*. 70 (2–3) (1995) 231-234.
25. P. Peyre, P. Merrien, P.H. Lieurade, and R. Fabbro, Laser induced shock wave surface treatment for 7075-T7351 aluminium alloys, *Surface Engineering*. 11(1), (1995) 47 – 52.
26. A. H. Clauer, Laser shock peening for fatigue resistance in surface treatment of titanium alloys, *The Metal Society of AIME Conference*. (1996) 217-230.
27. A K. Gujba and M Medraj, Laser Peening Process and Its Impact on Materials Properties in Comparison with Shot Peening and Ultrasonic Impact Peening, *Materials (Basel)*. 7(12) (2014) 7925–7974.

28. Y. Zhu, J. Fu, C. Zheng, Z. Ji Influence of laser shock peening on morphology and mechanical property of Zr-based bulk metallic glass, *Optics and Lasers in Engineering*, 74 (2015) 75 – 79.
29. D. Karthik and S. Sawroop Laser peening without coating—an advanced surface treatment: A review, *Materials and Manufacturing Processes*. 32(14) (2016), 1565 – 1572.
30. P.P. Shukla, .P.T Swanson, J.C. Page, Laser Shock Peening and Mechanical Shot Peening Processes Applicable for the Surface Treatment of Technical Grade Ceramics: A Review, *Proceedings of the Institution of Mechanical Engineers Part B: Journal of Engineering Manufacture*. 228(5) (2014) 639-652.
31. A. Koichi, S. Yuji, T. Kazuma T. Hiroto, I. O. Shin, Strengthening of Si₃N₄ Ceramics by Laser Peening, *Residual Stresses VII. ECRS7*, 524 – 525 (2006) 141-146.
32. G. J. Cheng, M. Cai, Daniel Pirzada, Maxime J.-F. Guinel, M. Grant Norton, (2008), Plastic Deformation in Silicon Crystal Induced by Heat-Assisted Laser Shock Peening, *Journal of Manufacturing Engineering*, 130, 011008-1 to 5.
33. P. Shukla, C. G. Smith, D.G. Waugh, J. Lawrence. Development in Laser Peening of Advanced Ceramics', *Proceedings of the SPIE*. 9657 (2015) 77-85.
34. P. Shukla and J. Lawrence, Laser Shock Peening of Si₃N₄ Ceramics: Experimental Set-up and General Effects. Science and Technology Facilities council (STFC) Annual Reports/article 2014/2015, P40.
35. P. Shukla and J. Lawrence, Alteration of Fracture toughness (K_{IC}) of Si₃N₄ Advanced Ceramics by Laser Shock Peening. Science and Technology Facilities council (STFC) Annual Reports/article 2014/2015, P41.
36. P. Shukla, S. Nath, W. Wang, X. Shen, J. Lawrence, Surface property modifications of silicon carbide ceramic following laser shock peening, *Journal of European Ceramic Society*. 37 (2017) 3027 – 3038.
37. P. Shukla, S. Robertson, H. Wu, A. Telang, M. Kattoura, S. Nath, S. R. Mannava, V. K. Vasudevan, and J. Lawrence, Surface Engineering Alumina Armour Ceramics with Laser Shock Peening, *Materials and Design*, 134 (2017) 523 - 538.
38. Shukla, P., Crooks, R., Wu. H., (2019), Shock-wave induced Compressive Stress in Alumina ceramics by Laser Peening, *Material and Design*, 167, 107626, 1-8.
39. F. Wang, C. Zhang, Y. Lu, M. Nastasi, and B. Cu, (2016), Laser Shock Processing of Polycrystalline Alumina Ceramics, *Journal of American Ceramic Society* (20 1–7 (2016).
40. Wang, F., Zhang, C., Yan, X., Deng, L., Lu, Y., Nastasi, M. & Cui, B. Microstructure-Property Relation in Alumina Ceramics during Post-Annealing Process after Laser Shock Processing. *Journal of the American Ceramic Society* (2018).

41. F. Wang, C. Zhang, X. Yan, L. Deng, Y. Lu, M. Nastasi, and B. Cui, Localized Plasticity in Silicon Carbide Ceramics Induced by Laser Shock Processing. *Materialia* 6 (2019), 100265.
42. T. Sekine, H. He, T. Kobayashi, M. Zhang, F. Xu, Shock-Induced Transformation of β -Si₃N₄ to a High-Pressure Cubic-Spinel Phase, *Applied Physics Letters* 76(25) (2000), 3706 – 3708.
43. K. SaiguS, K. TaKahaShi, and N. Sibuya, Evaluation of Surface Properties of Silicon Nitride Ceramics Treated with Laser Peening, *International Journal of Peening Science and Technology*, 1(3), 221 – 232.
44. Jean-Eric Masse, and Gerard Barreau, Laser Generation of stress-waves in metals, *Surface and Coatings technology*, 70 (1995), 231 – 234.
45. W. Pfeiffer, T. Frey, Advances in shot peening of silicon nitride ceramics, *Fatigue and Fracture of other materials* (2005) 326-331.
46. W. Pfeiffer, T. Frey, Strengthening of ceramics by shot peening, *Journal of the European Ceramic Society* (2006) 2639–2645.
47. P. Shukla, J. Lawrence Yu. Zhang, Understanding Laser-beam brightness: A Review on a New Prospective in Materials Processing, *Optics and Lasers in Engineering*, 75 (2015) 40 – 51.
48. D. Marshall and B. Lawn, An Indentation Technique for Measuring Stresses in Tempered Glass Surfaces. *Journal of the American Ceramic Society* 60(1-2) (1977) 86 - 87.
49. G. Quinn, G. Fracture Toughness of Ceramics by the Vickers Indentation Crack Length Method: A Critical Review. In: R. Tandon, A. Wereszczak and E. Lara-Curzio, ed., *Mechanical Properties and Performance of Engineering Ceramics II: Ceramic Engineering and Science Proceedings*, 27 (2006) Hoboken: John Wiley & Sons.
50. F. Rickhey, K. Marimuthu, and H. Lee Investigation on Indentation Cracking-Based Approaches for Residual Stress Evaluation. *Materials* 10(4) (2017) 404.
51. C.B Ponton and R.D. Rawlings, Vickers indentation fracture toughness test, Part 1 – Review of literature and formulation of standardised indentation toughness equations. *Mater. Sci. Technol.* 5 (1989) 865–872.
52. P.P Shukla, J. Lawrence, Fracture toughness modification by using a fibre laser surface treatment of a silicon nitride engineering ceramic. *Journal of Materials Science* 45 (23) (2010) 6540-6555.
53. I. J. McColm, *Ceramic hardness*, 1990, (UK, University of Bradford, New York, Platinum Press).
54. P.P. Shukla, J. Lawrence, Examination of temperature distribution on silicon nitride engineering ceramics during fibre laser surface treatment. *Optics and Lasers in Engineering*. 49 (7) (2011) 998 – 1011.

55. [55] O. Hesse, J. Merker, M. Brykov, V. Efremenko*, Aus Wissenschaft und Forschung, (2013), Abrasive wear resistance of high-carbon low-alloy steels, Tribologie und Schmierungstechnik 60(6), 37-43.
56. S. Prabhakaran, S. Kalainathan, P. Shukla, V.K. Vasudevan, Residual stress, phase, microstructure and mechanical property studies of ultrafine bainitic steel through laser shock peening. Optics and Laser Technology. 115 (2019) 447 - 458.

Graphical Abstract

